Introduction

Many factors influence hydrodynamic behavior in CFBR. The inlet and exit configuration, particle size and distribution, solid concentration, pressure, and particle properties such as cohesiveness play important roles in determining flow behavior. The hydrodynamics of gas and solids have a significant impact on heat transfer, reaction kinetics, and catalyst activity. In this study we are interested in the flow patterns in the riser part of a CFBR. Therefore, in the computational space domain there are initial conditions and physical boundaries consisting of wall boundaries, an inflow boundary, and an outflow boundary.

Development of the CFD Domain

Two pipe-elbow configurations, called Riser I and Riser II, are used to model the riser section of a CFBR system. Each of these two models is comprised of an inlet, an exit, a pipe and connecting elbows. Riser II has a longer inlet and main pipe sections compared to Riser I to allow for scrutinizing the effects of riser dimensions on flow properties. GAMBIT, the Graphical User Interface (GUI) included in the FLUENT commercial software package is used for generating the geometrical models of these two computational domains.

Riser I Configuration

Figure 1 shows the cylindrical two-dimensional pipe-elbow system that is used for the initial study of the riser's gas-solid two-phase flow. The inlet and exit sections are 0.1 m in length, each. The pipe diameter is 0.1 m and its height is 1.4 meters. The inlet and exit are connected to the pipe with 90° elbows. The gas-solid flow enters the system from the lower left part (Inlet) of the riser and exits to top right (Exit).

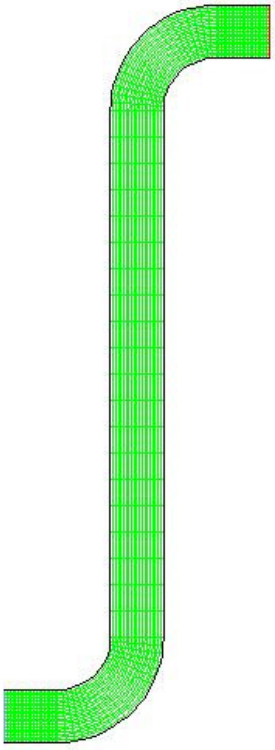

Figure 1. Riser I configuration

This system was meshed with two methods: quadratic and triangular meshes to extract the effects of spatial discretization type on simulations. The number of cells for the quadratic mesh model is 2000 while the triangular mesh has 6683 cells. The numbers of nodes are 2121 and 7049 for the quadratic and triangular meshes, respectively. Figure 2 shows the inlet section of the system with quad (Fig. 2a) and triangular (Fig. 2b) mesh types.

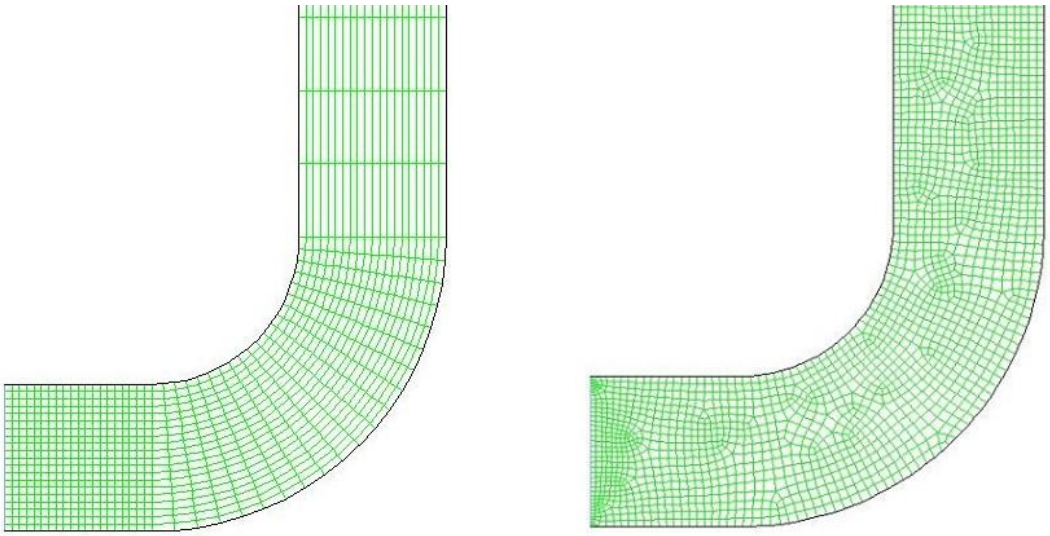

(a) (b)

Figure 2. Models meshed with quad (a) and triangular (b) cells

Riser II Configuration

The second configuration model, shown in Fig. 3, has the same diameter as that of Riser I. However, the inlet section of the pipe was elongated to 0.7 meters to study the inlet effects on riser flow. The height of the riser pipe is also extended to 3.0 meters in this configuration.

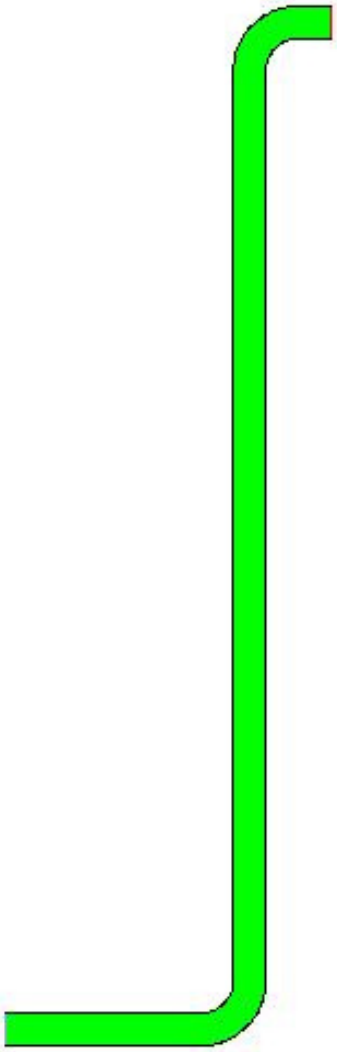

Figure 3. Riser II Configuration

The Riser II configuration is meshed with quad cells for the inlet and exit, and pipe sections while triangular cells are used for the two elbow sections. This design is intended for better visualization of flow dynamics in elbow sections and to gain experience with grid generation of mixed cell type meshing technique. The total mesh has 15,901 nodes, 33700 faces, and 17800 cells with 1 cell and 5 face zones. Cell types and

their distribution are visible in Fig. 4. To enhance accuracy and resolution of flow physics, finer cells are placed along the boundary layers for inlet, exit, and riser pipe section, while unstructured triangular meshes filled in the elbow sections.

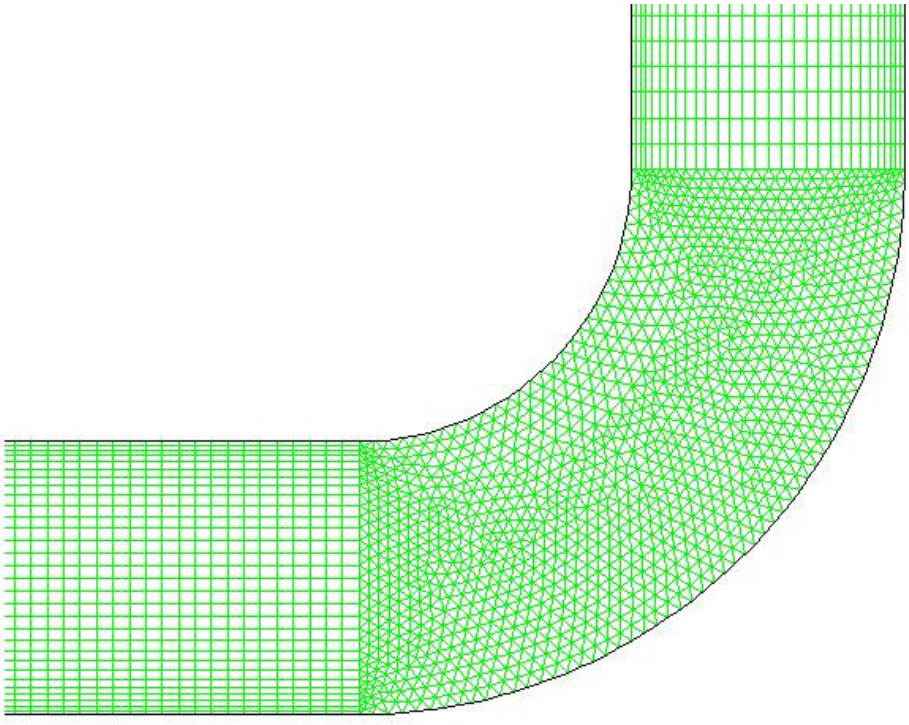

Figure 4. Triangular meshes are placed in elbow sections and quad meshes are used for the remainder of the riser domain

Operating Conditions and Solver Settings

Each model was simulated for both steady state and transient conditions. FLUENT computational solver settings are summarized below. The complete information generated by the FLUENT solver is given in the appendix of this report.

<u>Condition and Setting for Riser I</u>

[Boundary Conditions]

Inlet: Velocity Inlet, Air=10.0m/s, Solid Particle=9.0m/s

Exit: Pressure Outlet, Gauge Pressure=0.0 pascals

Solid particle volume fraction: 0.1

Wall roughness: 0.0 mm

[Material]

Air density: 1.225 kg/m^3

Solid particle bulk density: 817.0 kg/m^3

Solid particle mean diameter: 1e-05 m

[Solver Setting]

Pressure based N-S equation solver

2D Implicit formulation

Eulerian 2-phase model

κ–ε viscous model

Condition and Setting for Riser 2

[Boundary Conditions]

Inlet: Velocity Inlet, Air =5.0 m/s, Solid Particle = 2.0m/s

Exit: Pressure Outlet, Gauge Pressure=0.0 pascals

Solid particle volume fraction: 0.2

Wall roughness: 0.0 mm

[Material]

Air density: 1.225 kg/m^3

Solid particle bulk density: 2200.0 kg/m^3

Solid particle mean diameter: 1e-04 m

[Solver Setting]

Pressure based N-S equation solver

2D Implicit formulation

Eulerian 2-phase model

κ–ε viscous model

Results and Discussions

Riser-I

Steady State Simulations

A steady state model with triangular meshes was used to simulate the two phase flow in the CFBR riser. The numerical simulations yielded the distributions of static pressure, velocity magnitude, and volume fraction of the two-phase gas-solid turbulent mixtures within the riser section. The turbulence intensity of the system was closely monitored during and after the computation.

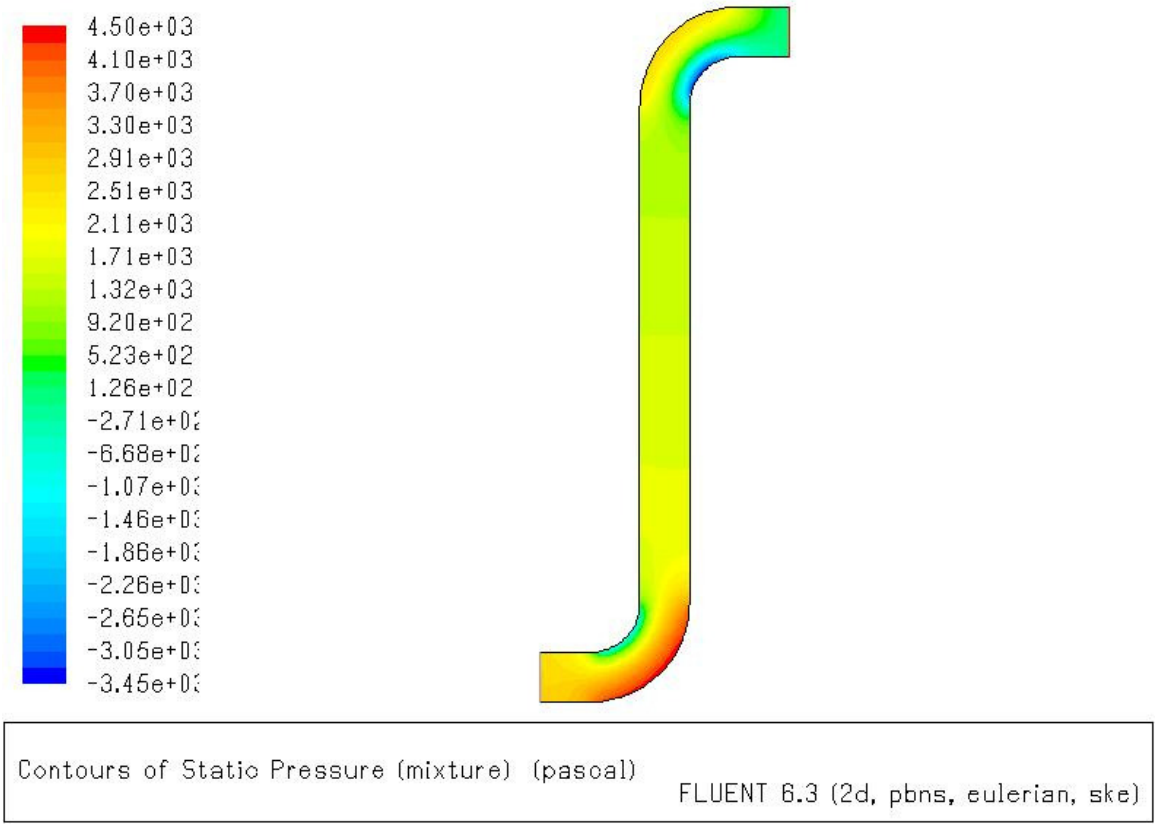

Figure 5. Contours of mixture static pressure (Pa)

Figure 5 indicates that the highest and lowest pressures in the riser occur in the outer and inner surfaces of the elbows due to the flow acceleration and deceleration, respectively. The high pressure gradient in the elbows correspond to a large pressure drop associated with flow separation which is a main concern in particle conveyor systems in general since it may lead to erosion of elbow material and increase in power demand for flow circulation.

Figure 6 manifests the contours of air velocity through the riser. A uniform inlet air velocity of 10 m/s was prescribed at the riser inlet. The entrance length was not long enough for the influx of air velocity profile to become fully developed. The maximum velocity magnitude of 13.4 m/s was reached at the curving elbow sections. This is mainly due to the Newtonian and no-slip boundary conditions characteristics of the flow. Noticeable detachment regions of the boundary layer are present signifying the flow separation alluded to in relation with Fig. 5.

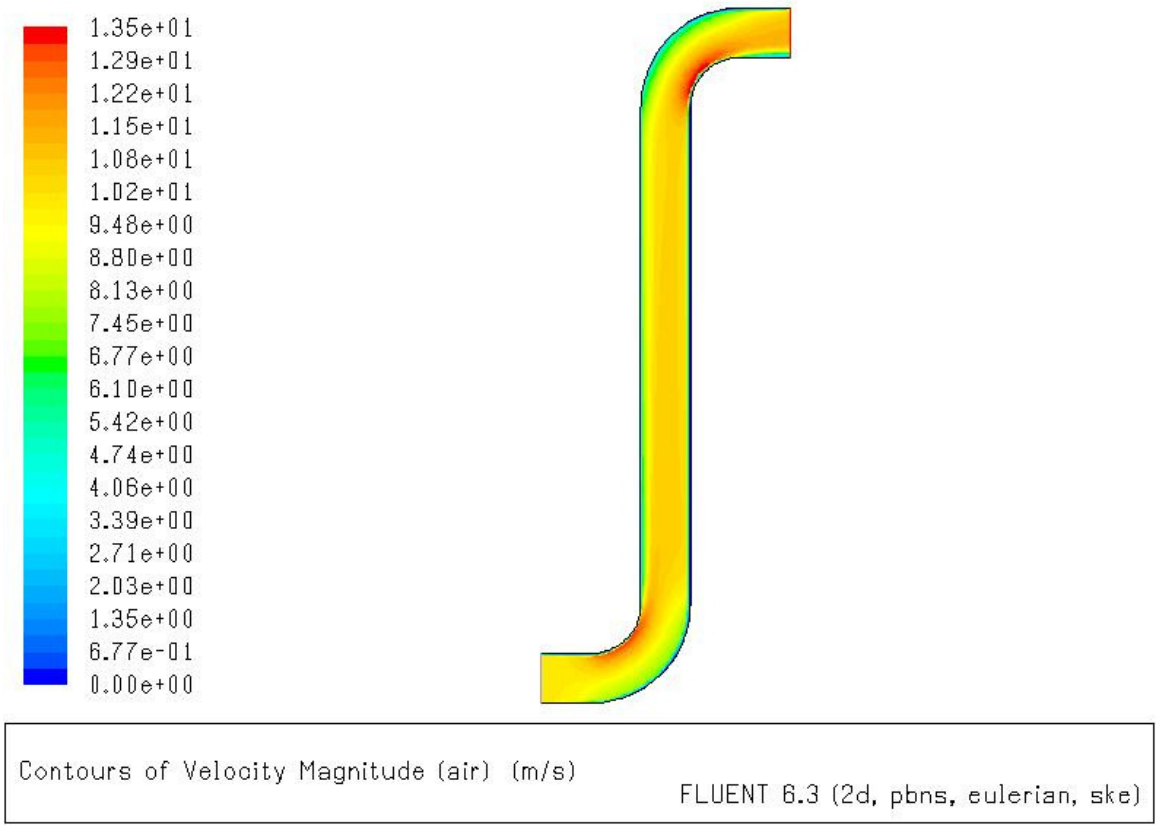

Figure 6. Contours of velocity magnitude for air

Since the bulk density of the solid particles is 667 times bigger than that of air, the inertia of solid particles is not sufficient to keep the particles dispersed in the air stream. Particles deposition on riser surfaces takes place, particularly at the low velocity regions that subsist at the bends of the elbow sections, which is clear in Fig. 7.

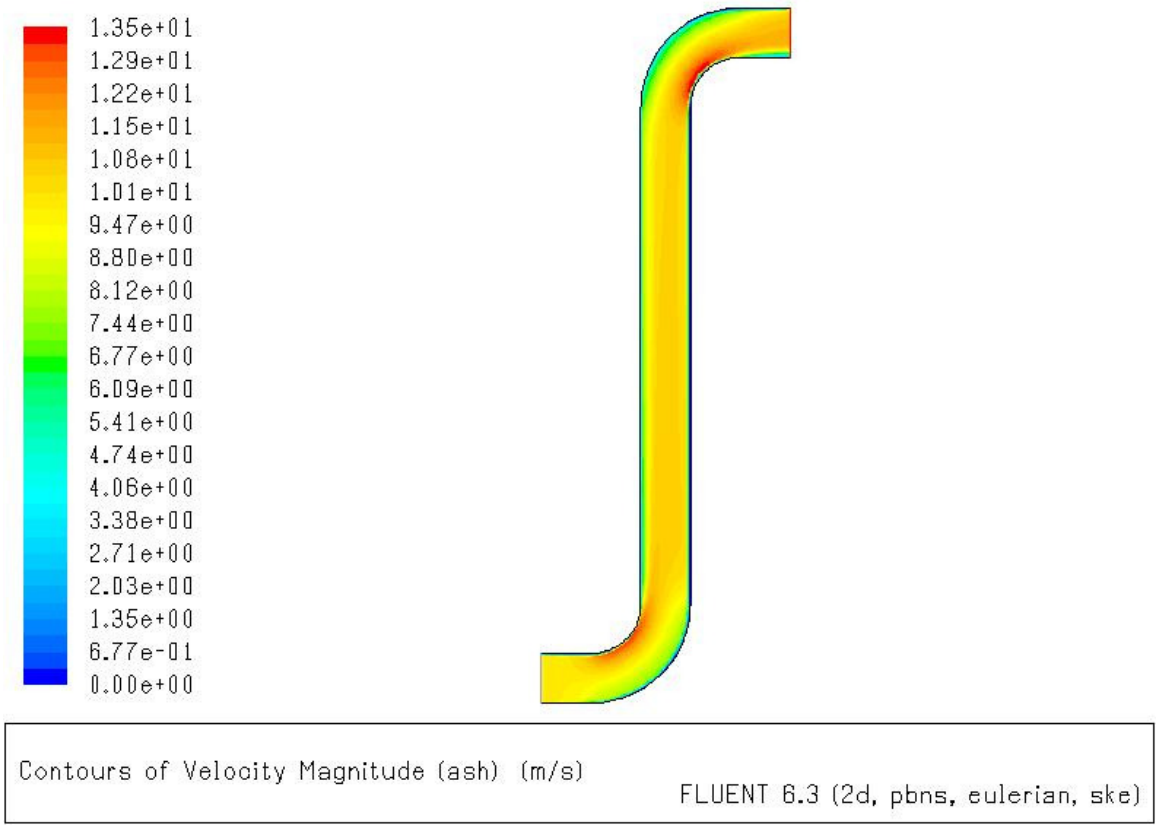

Figure 7. Contours of velocity magnitude for solid particles

Figure 8 explicates the solid particles volume fraction in the two-phase system. The inlet volume fraction of the solid particles was prescribed as 0.1. Since there are sharp pressure and velocity gradients at the elbow bends, the particles traveling with air start to separate from air and accumulate. Inertia differences between air and solid particles exhibit the most prominent effect at these regions.

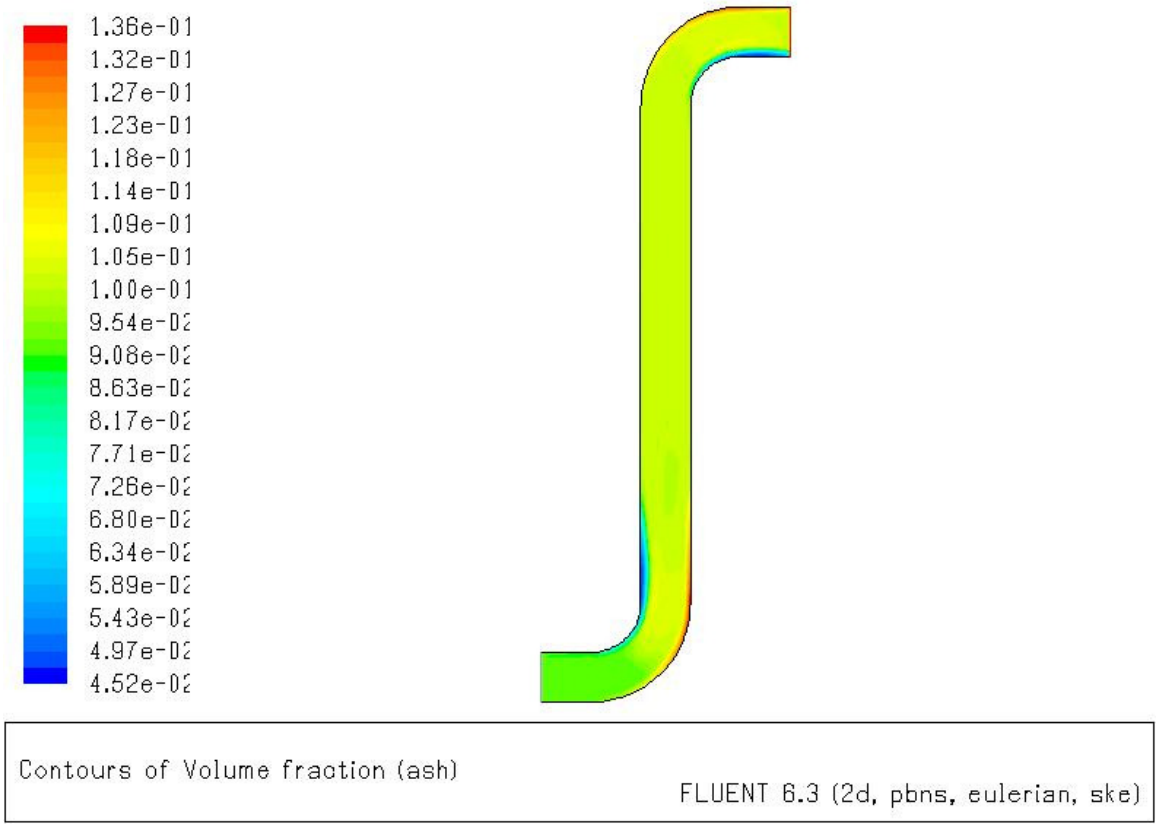

Figure 8. Contour of solid particle volume fraction. The highest volume fraction regions coincide with lowest velocity magnitude regions.

The mass flow rates of air and solid particles were computed and listed in Table 1. The net mass flow rate has a negative value of 7.9 kg/s: mass leaving the system has bigger value than that of inlet. This is not possible under a single phase, incompressible flow scenario. However, for the present two-phase gas-solid simulations a 'flush-out' phenomenon of the particles accumulated in the system leads to mass flow rate fluctuations with time. Since steady state simulation provides time-averaged solutions, it is plausible that the mass flow rate of exiting solid particles may fluctuate.

Table 1. Mass flow rates (kg/s)

Inlet	74.633
Exit	-82.558
Net	-7.925

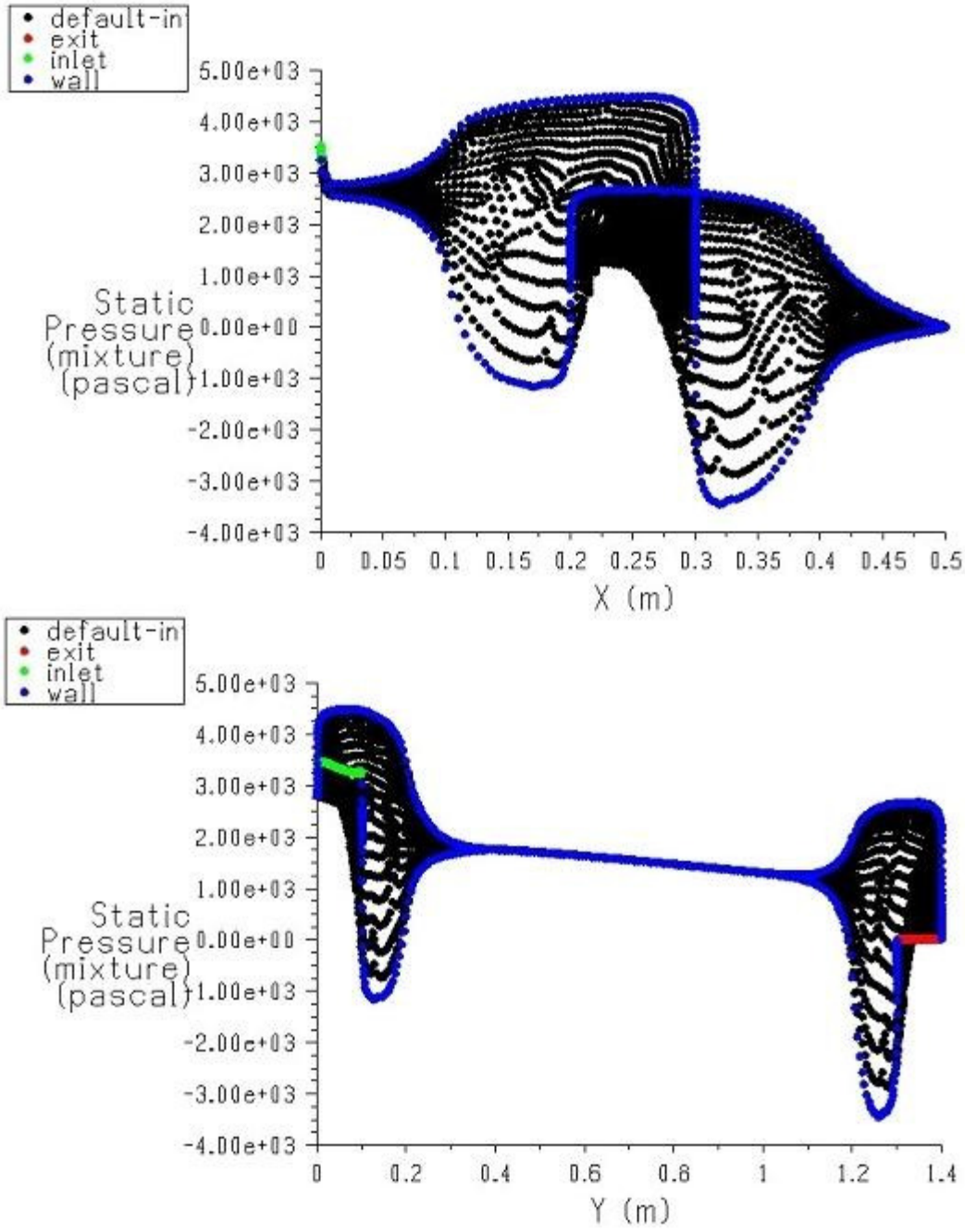

Figure 9. Static pressure of the mixture along horizontal (X) and vertical (Y) axes

The X-Y plot of static pressure of the mixture versus system length, Fig. 9, reveals that the mixture pressure gradients are largest in the elbow sections which coincides with the behavior of static pressure clarfied in Fig. 5.

Figure 10 shows the Turbulence Kinetic Energy (TKE) of the air in the system. Although air flow is fully developed, the TKE has non-symmetrical distribution in a horizontal cut planes through the riser section. It is believed that the heavier solid particles are slipping from the transporting air stream in this region which causes an uneven TKE distribution. This observation is in accord with the assumption of slip ratio in the vicinity of 0.9 generally prevalent in the literature.

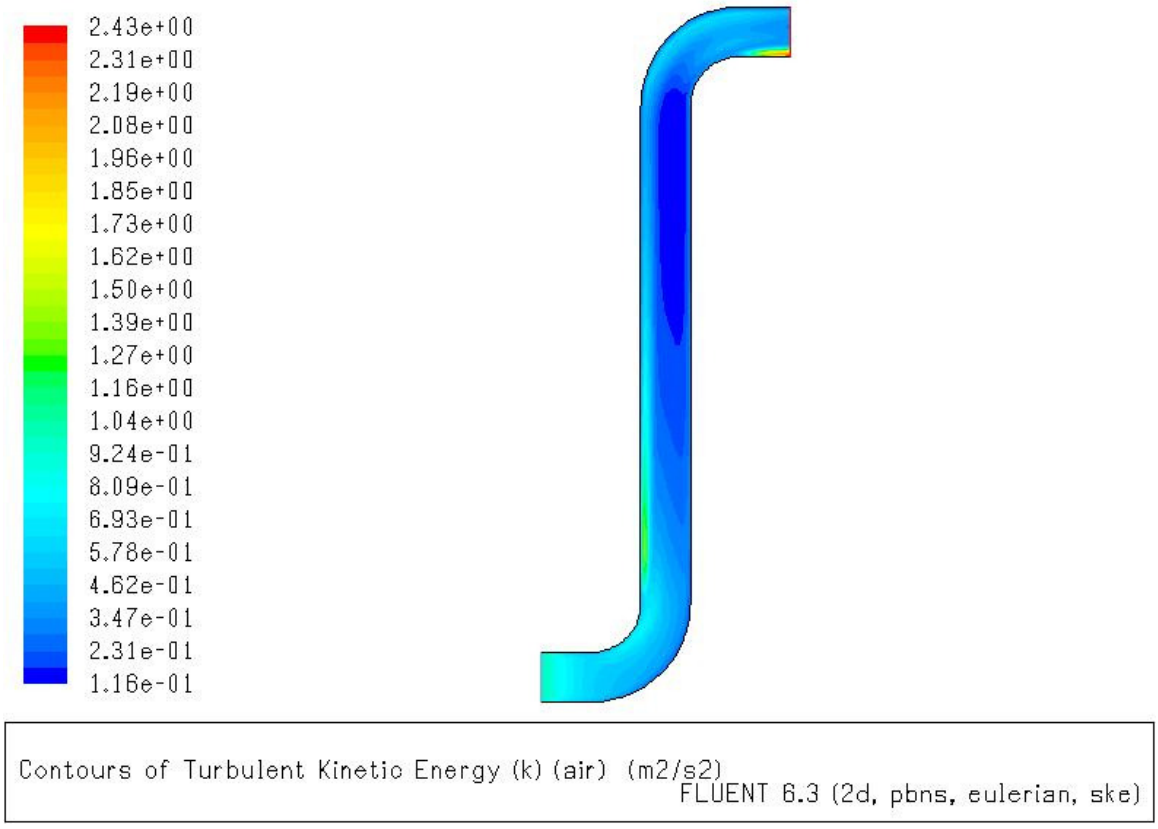

Figure 10 Contours of Turbulent Kinetic Energy (TKE) for air in the system

Unsteady State Simulations

While steady state simulations provide time-averaged quantities of the flow properties, unsteady state computations reveal accurate flow variations with time. Applying the same flow properties and boundary conditions used in steady state analyses, time marching solutions were obtained and analyzed. The time step between iterations was chosen as Δt = 0.00025 seconds, and the maximum number of iterations to achieve convergent solution at each time step was set at 20.

Figure 11 shows the static pressure distributions in the riser section at time steps of 1.5, 1.5, and 2.5 seconds from left to right, respectively. The differences are too minute in these time steps to observe any dynamic changes in static pressure contours. However, there is an apparent pressure smoothing-out process taking place in the elbows.

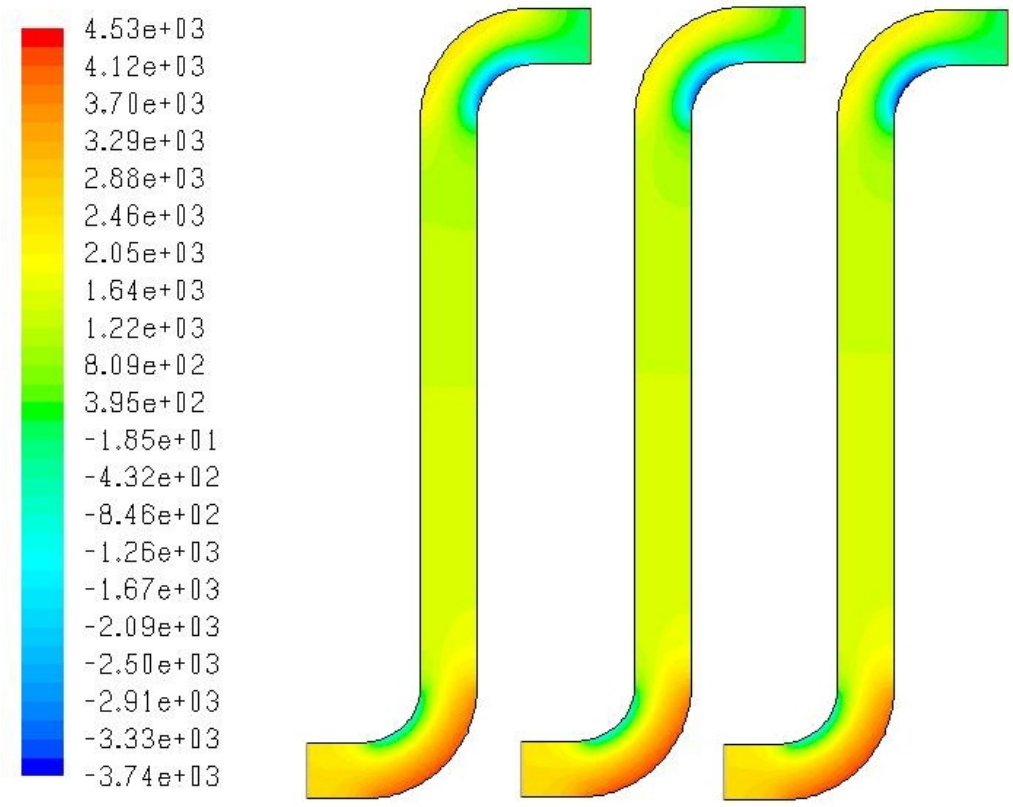

Figure 11. Contours of static Pressure for the mixture (Pa)
Time steps = 0.5, 1.5, and 2.5 seconds from left to right.

At the early stages of flow development, around 1/1000~1/100 seconds for example, flow property changes are measurably intense. However, solutions at that early stage are purely mathematical thus has no importance in physics of fluid flow. As time progresses from 0.5 to 2.5 seconds little differences are distinguishable in the static pressure distribution and it is deduced that the flow is rapidly established exhibiting steady-state-like fluid dynamics. This remark is also applicable to the velocity magnitude of the solid particles shown in Fig. 12.

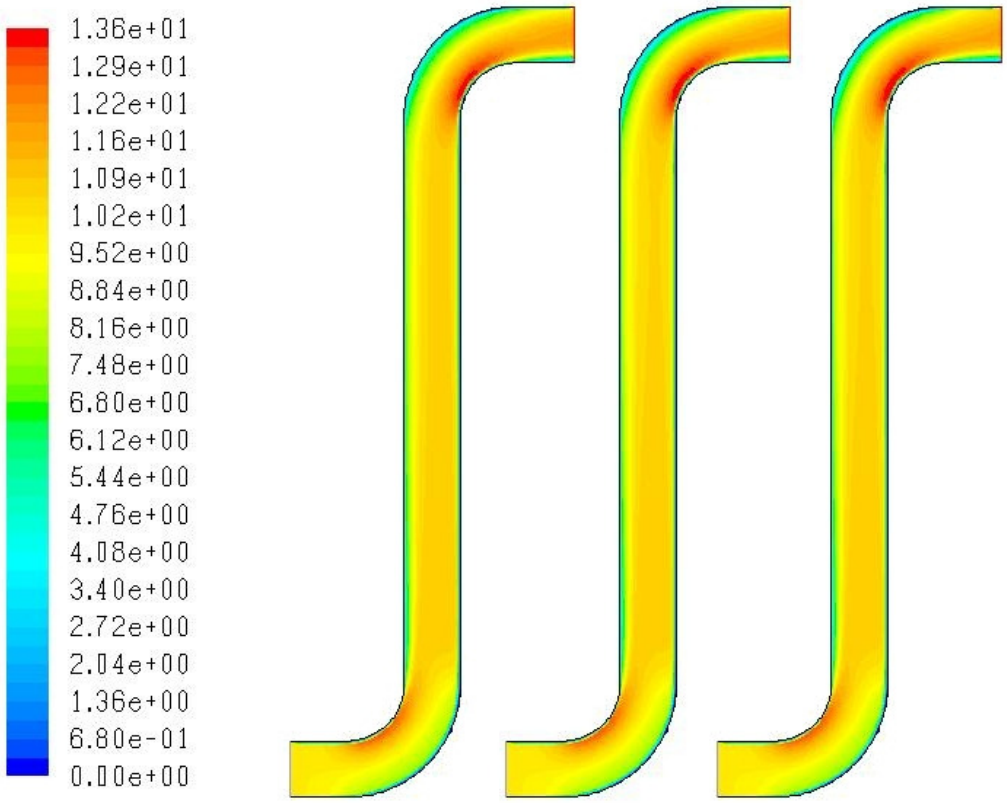

Figure 12. Contours of velocity magnitude for Solid particles (m/s)
Time steps = 0.5, 1.5, and 2.5 seconds from left to right.

Figures 13 ad 14 present the contours of volume fraction for solid particles and Total Kinetic Energy (TKE) for air, respectively, at time steps of 0.5, 1.5, and 2.5 seconds from left to right. The results are indistinguishable from the steady state solutions, and also time changes in each time steps are to minuscule to be noteworthy. This implies, for this

geometry and flow conditions, that steady state analyses would be adequate enough to model the flow.

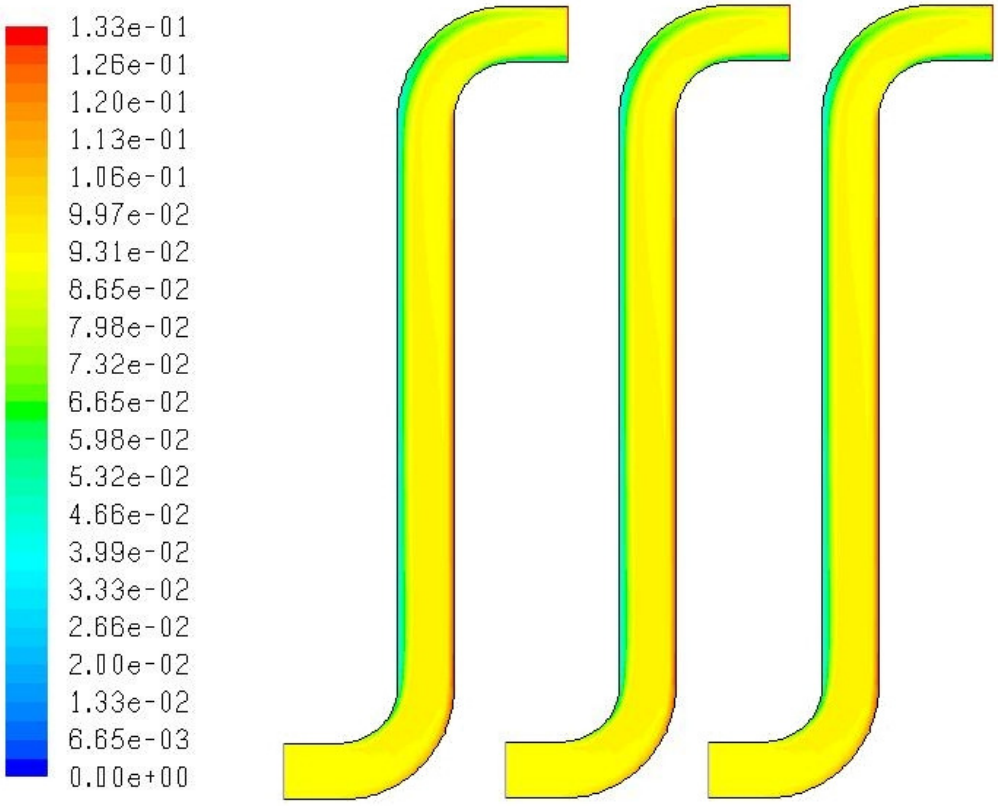

Figure 13. Contours of volume fraction for solid particles
Time steps = 0.5, 1.5, and 2.5 seconds from left to right.

In Table 2 the mass flow rates of air-particles for the unsteady state system are listed at time = 2.5 seconds. The net mass flow rate is -0.25 kg/s: when compared to the steady state net mass flow rate (-7.9 kg/s), the unsteady flow seems well stabilized.

Table 2. Surface flux computation: Mass Flow Rates (kg/s)

Inlet	74.632
Exit	-74.878
Net	-0.246

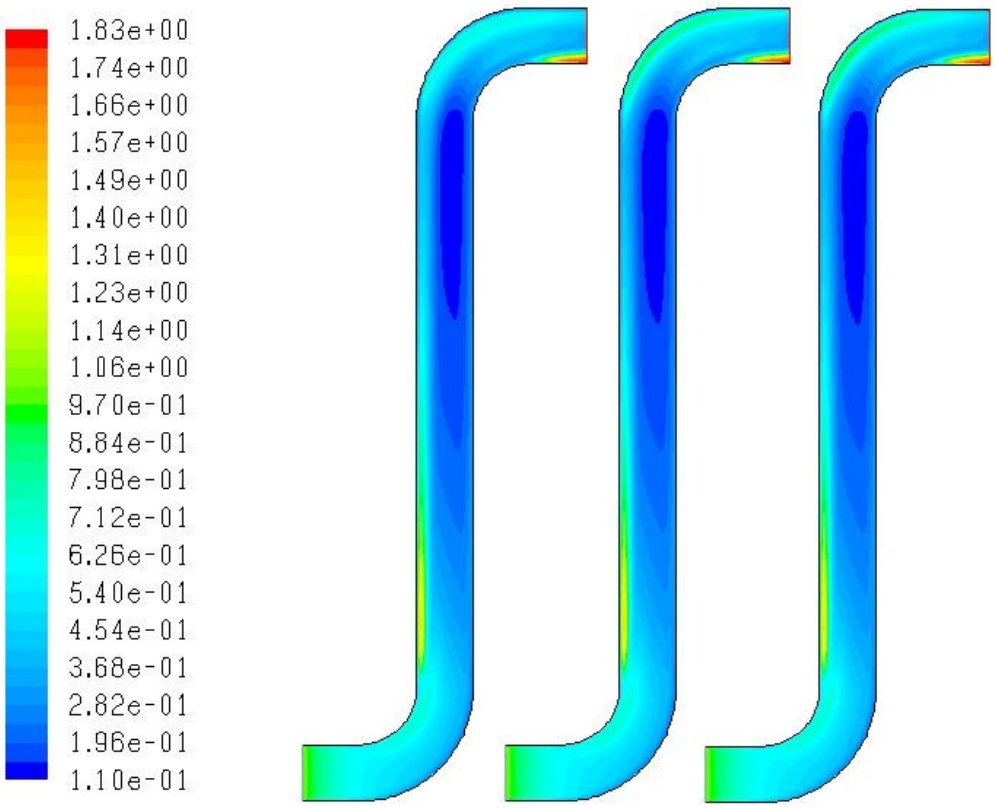

Figure 14. Contours of Turbulent Kinetic Energy (TKE) for air (m^2/s^2)
Time steps = 0.5, 1.5, and 2.5 seconds from left to right.

The pressure drop along the pipe system is plotted in Figure 15. It is seen that the results obtained are very similar to those of the steady state case.

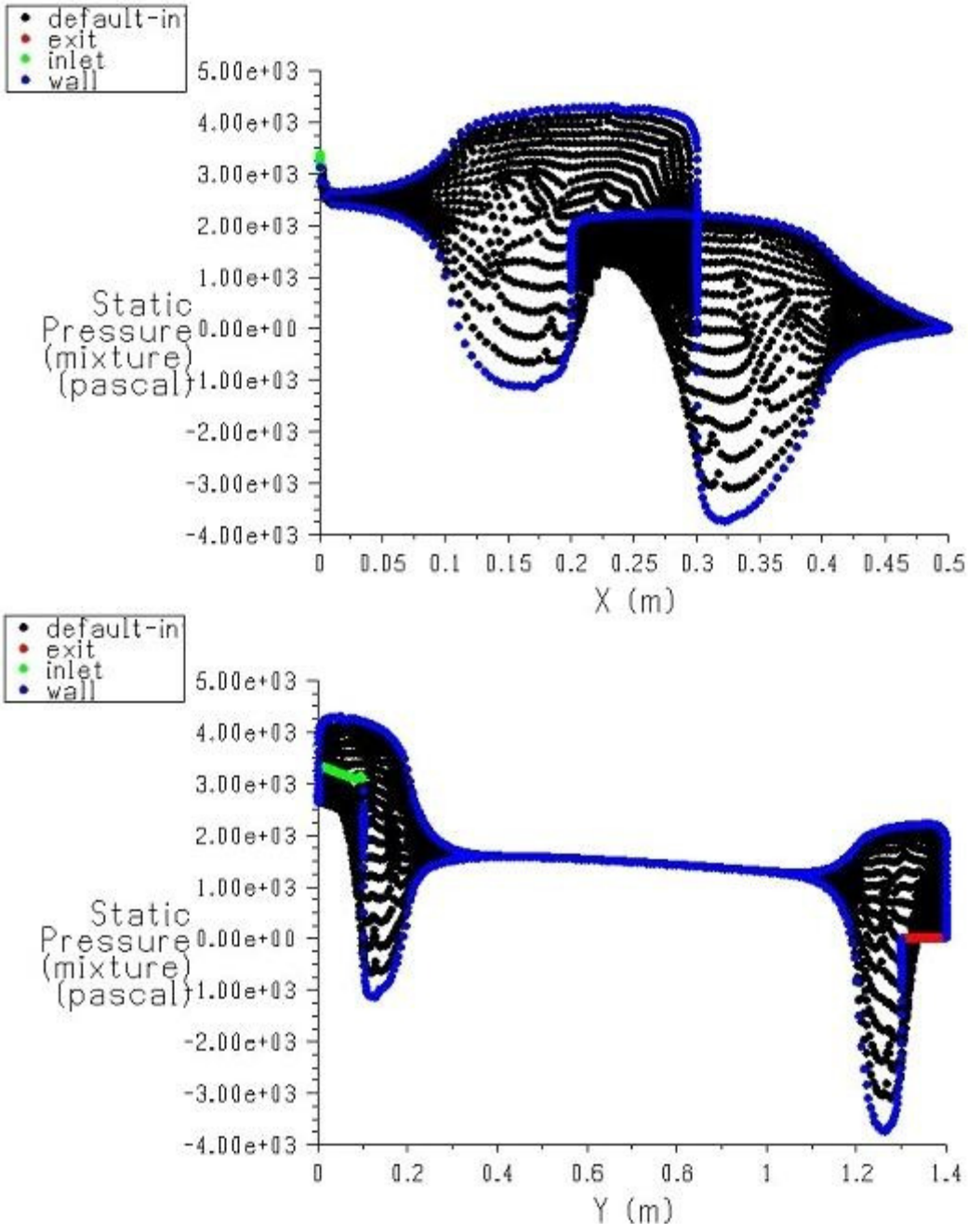

Fig. 15. Static pressure of the mixture along horizontal (X) and vertical (Y) axes

Riser-II

The solid particles considered in the Rise II configuration are 2.7 times heavier than that considered in Riser-1 simulations with particle bulk densities of 2,200 and 817 kg/m^3, respectively. The same type of initial and boundary conditions were applied for both steady and unsteady computations. The inlet velocities of air and particles were set at 5.0 and 2.0 m/s, respectively.

Steady State Simulations

The numerically obtained contours of static pressure in the riser are depicted in Fig. 16. The static pressure of mixture at the inlet surface was computed from the inlet velocities to be 19.4 kPa. It is seen that the pressure drop in the inlet pipe is initially linear then followed by an oscillatory behavior in the riser's vertical pipe. As was pointed out and discussed with the Riser-I model, a sharp pressure gradient persist at the elbows' bend. This sudden pressure variation propagates and dissipates through the vertical section, resulting in pressure fluctuations. It is believed that the main cause of the pressure fluctuations is the instability of the steady state iteration methods. Multi-phase flow systems are inherently unstable, thus the system characteristics are very time dependent. This becomes even more realized for a system with higher solid phase density and velocity slip ratio. Riser I simulations did not exhibit much instability due to employing a particle/air inlet velocity slip ratio of 0.9. The slip velocity for Riser-II is calculated from the ratio of particles to air inlet velocities as 2/5 = 0.4. It is also worth noting that solving a very strongly time dependent problem with steady state methods may not be possible in some multiphase flow cases. Even when iterations appear to satisfy convergence criteria, the solution suffers from instabilities.

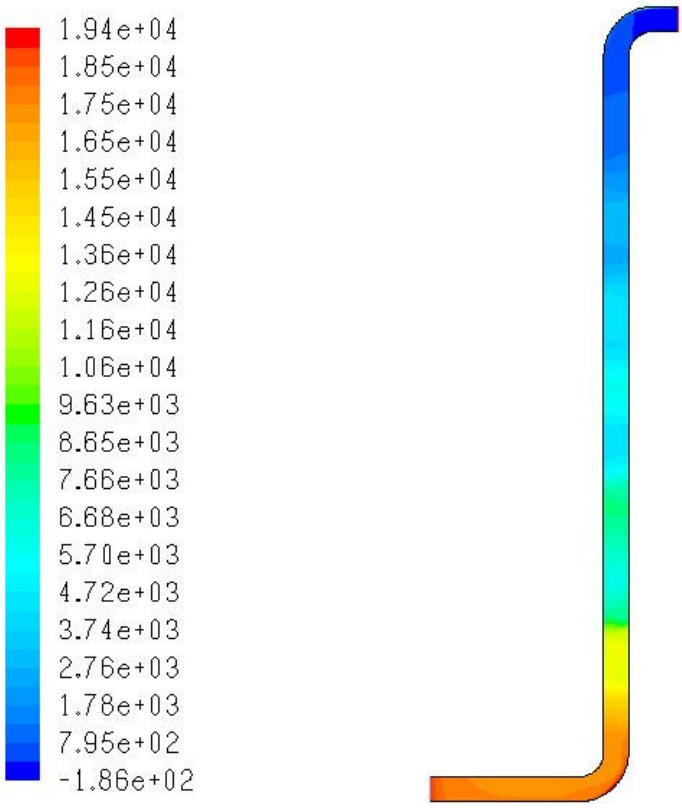

Figure 16. Contours of static pressure of air-solid particle mixture in (Pa)

The static pressure variation of the mixture along the riser is graphed in Figure 17. The pressure drop in the horizontal section is small compared to that in the vertical section. High pressure gradients are experienced by the flow as the mixture goes through the elbow sections due to directional momentum change and pressure oscillations.

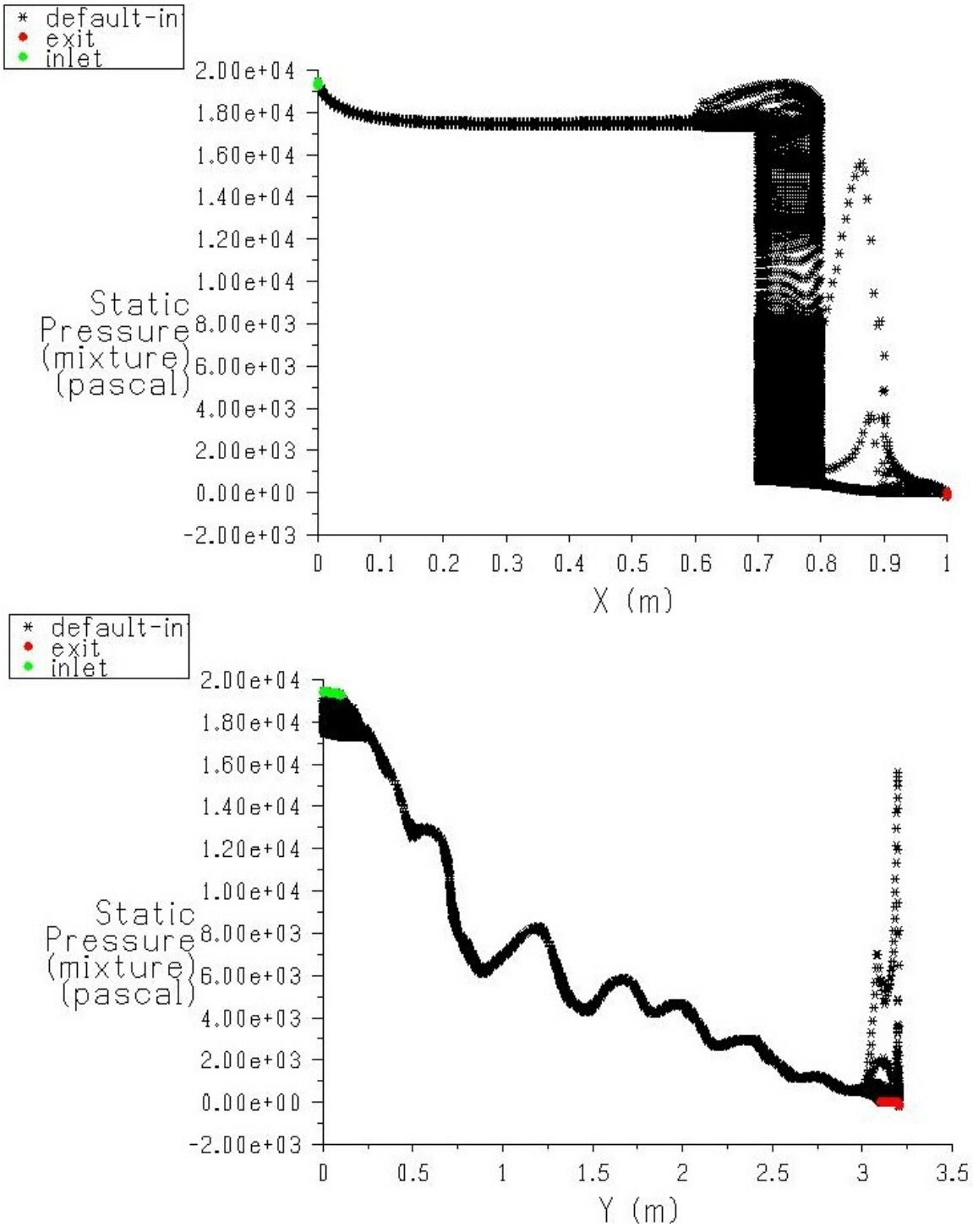

Figure 17. Static pressure of the mixture along horizontal (X) and vertical (Y) axes

The velocity magnitude of air in the system is portrayed in Fig. 18. At the inlet surface, the normal-to-boundary air velocity is 5.0 m/s. As the air-particle mixture flows into the inlet pipe, a fully developed pipe flow profile is formed, in about three diameter distance from the inlet, and the maximum magnitude of velocity reaches 8 m/s. This profile is disrupted when the flow reaches the inlet elbow section. The sudden change of flow direction that takes place in the elbows brings about velocity fluctuations and oscillations as evident from the velocity pattern in the elbow sections. As with pressure fluctuations, the cause for this uneven flow pattern is mainly due to high particle/air density ratio and the inherent instability of the steady state solution. The oscillation of velocity magnitudes coincides with that of pressure, that is, where pressure reaches local minimum values of velocity achieve local maximum. This is a typical behavior of inviscid, incompressible flow as can be explained with the Bernoulli's equation.

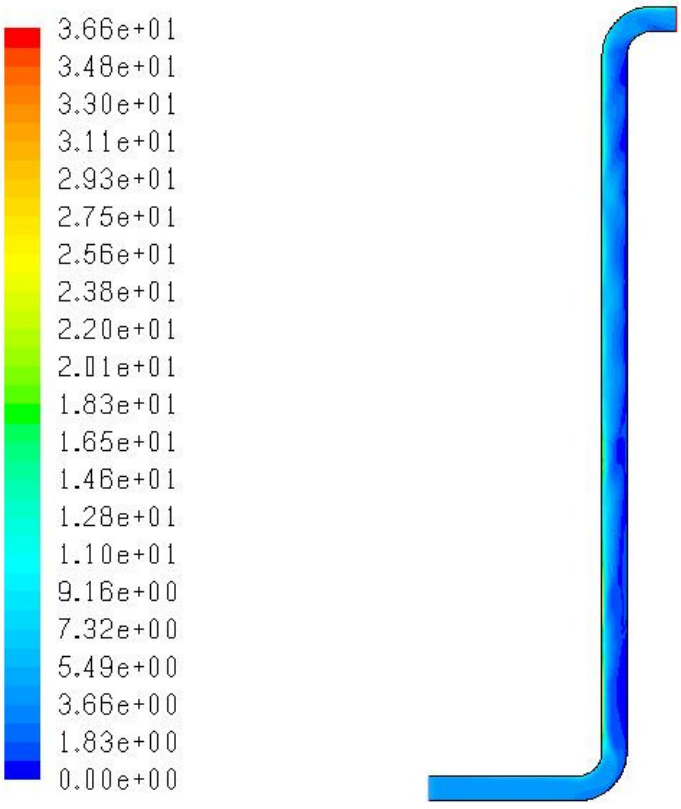

Figure 18. Contour of velocity magnitude for air (m/s)
The uneven velocity distribution resulting in fluctuations in pressure is visible.

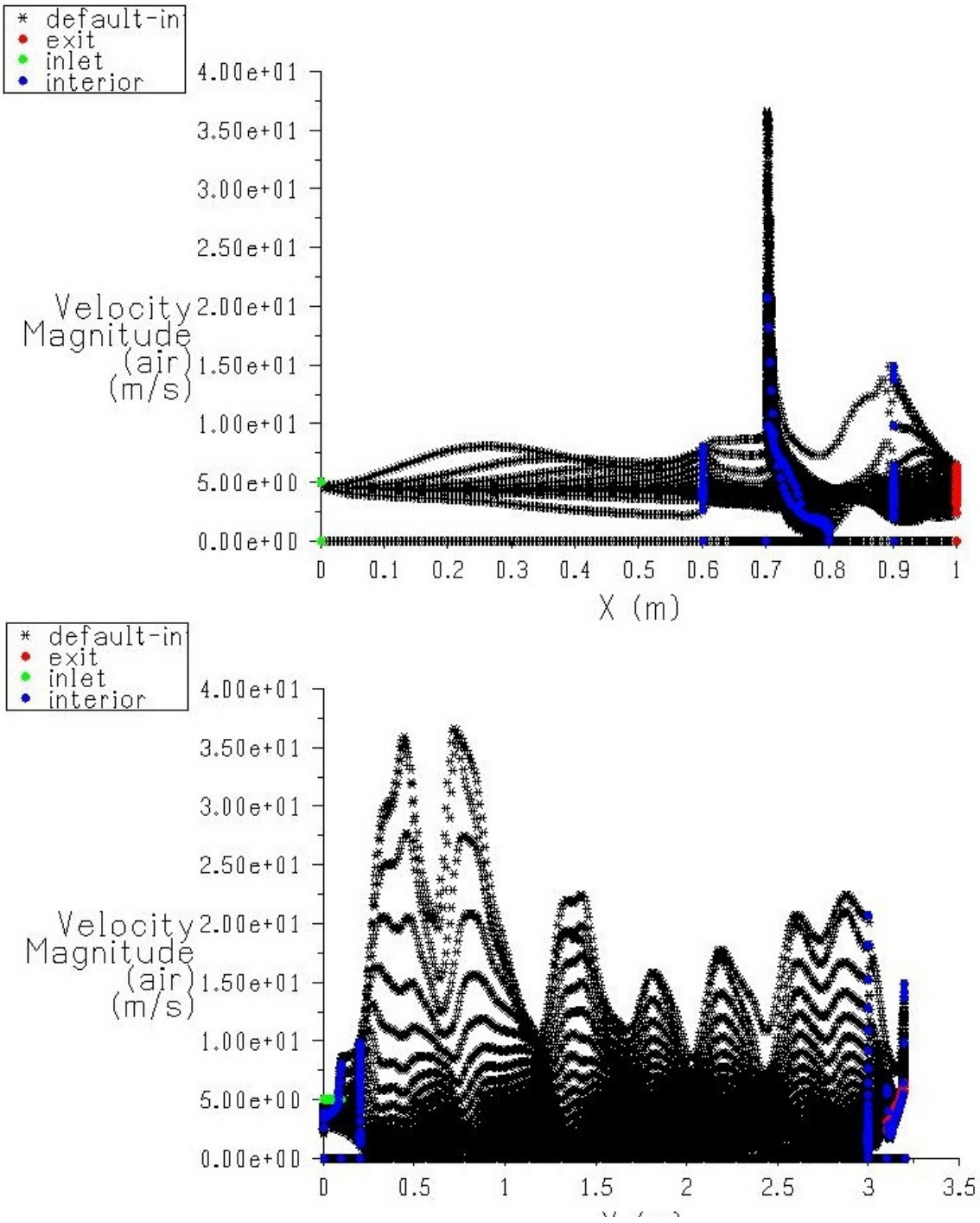

Figure 19. Velocity magnitude of air along horizontal (X) and vertical (Y) axes

As the solid particles enter the elbow leading to the vertical section of the riser, the influence of gravitational forces become more pronounced. The loss of energy due to flow separation in the elbows aided by gravitational effects cause the heavy solid particles to accumulate at the outer surface of the lower elbow as inferred from Fig. 20. With energy transferred from air stream, particles move upward. There is a balance between particle bulk motion and gravity with frictional force, which leads to oscillations of the entire air-particle mixture flow. The highest volume fraction region is located at the vertical pipe immediately after the inlet elbow section. This high density region works as storage space for the incoming particles, intermittently releasing over stocked particles to downstream thus generating the aforementioned fluctuating flow pattern.

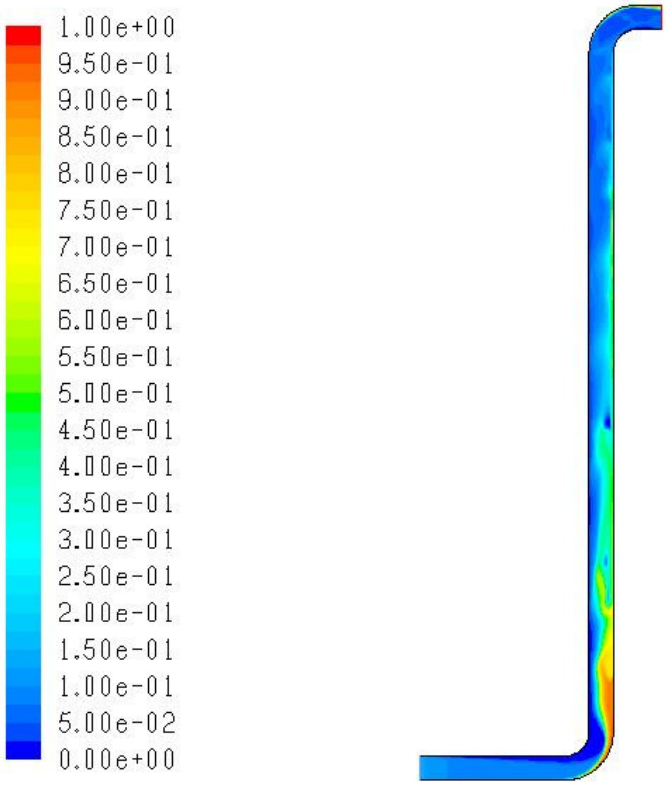

Figure 20. Contours of particle volume fraction in the system
High volume fraction regions develop along the pipe wall surface.

Mass flow rates at the riser inlet and exit are computed and tabulated in Table 2. The solid particles contribute to most of the mass in the flow system; mass ratio of air/particle at inlet is 5.6e-03. There is a noticeable mass imbalance in the system with net mixture mass rate of -98.3 kg/s. This is believed to be unrealistically high although fluctuation of mass flow rate at the exit is expected. As discussed earlier with the pressure and velocity results, the steady state solution of the flow lacks accuracy. However it is possible to discern the main flow features from via steady state computations which have the advantage of requiring significantly shorter simulation times compared to the more realistic unsteady state solutions.

Table 3. Surface flux computation: Mass Flow Rate (kg/s)

	Mixture	**Air**	**Particle**
Inlet	88.4900	0.4900	88.0000
Exit	-186.7884	-0.4358	-186.3527
Net	-98.2984	0.0542	-98.3527

Unsteady State Simulations

Unsteady state solution sets were generated with similar operation and boundary conditions as those of steady state solution. However, the unsteady state solutions were capable of capturing time dependent physical phenomena that were not possible to identify by the steady state solution.

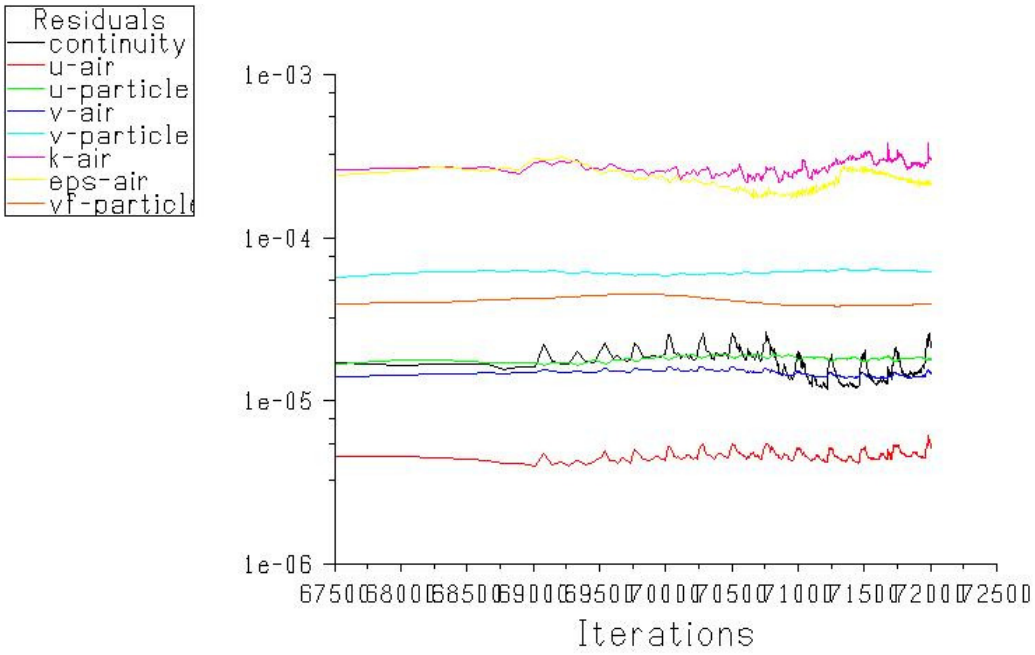

Figure 21. Monitoring residuals for convergence of the solution

Since convergent iterations in unsteady state mode critically depends upon the successful choice of time step size, several time steps had to be tested before deciding on a time step of $\Delta t = 0.00025$ seconds for the present simulations. The maximum number of iterations at each time step was set at 50. The time marching numerical solution scheme did not require more than 3~4 iterations for convergence. The residual monitoring process results reported in Fig. 21 indicate that a stable and convergent solution was promptly achieved. The convergence criterion for each variable was set at 0.001.

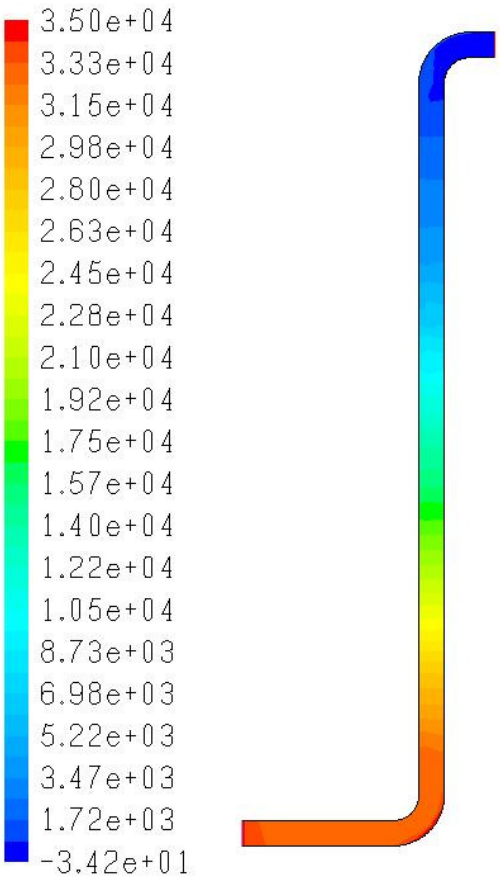

Figure 22. Contours of static pressure of air-solid particle mixture (Pa) at 15.0 sec

Although initial oscillations in flow quantities were observed, the solution stabilized after about 2.0 seconds. At the time of 15.0 seconds the pressure drop for the unsteady state system was ΔP= 34.3kPa which is 1.8 times larger than that of the steady state solution which correlates with time-averaged quantities.

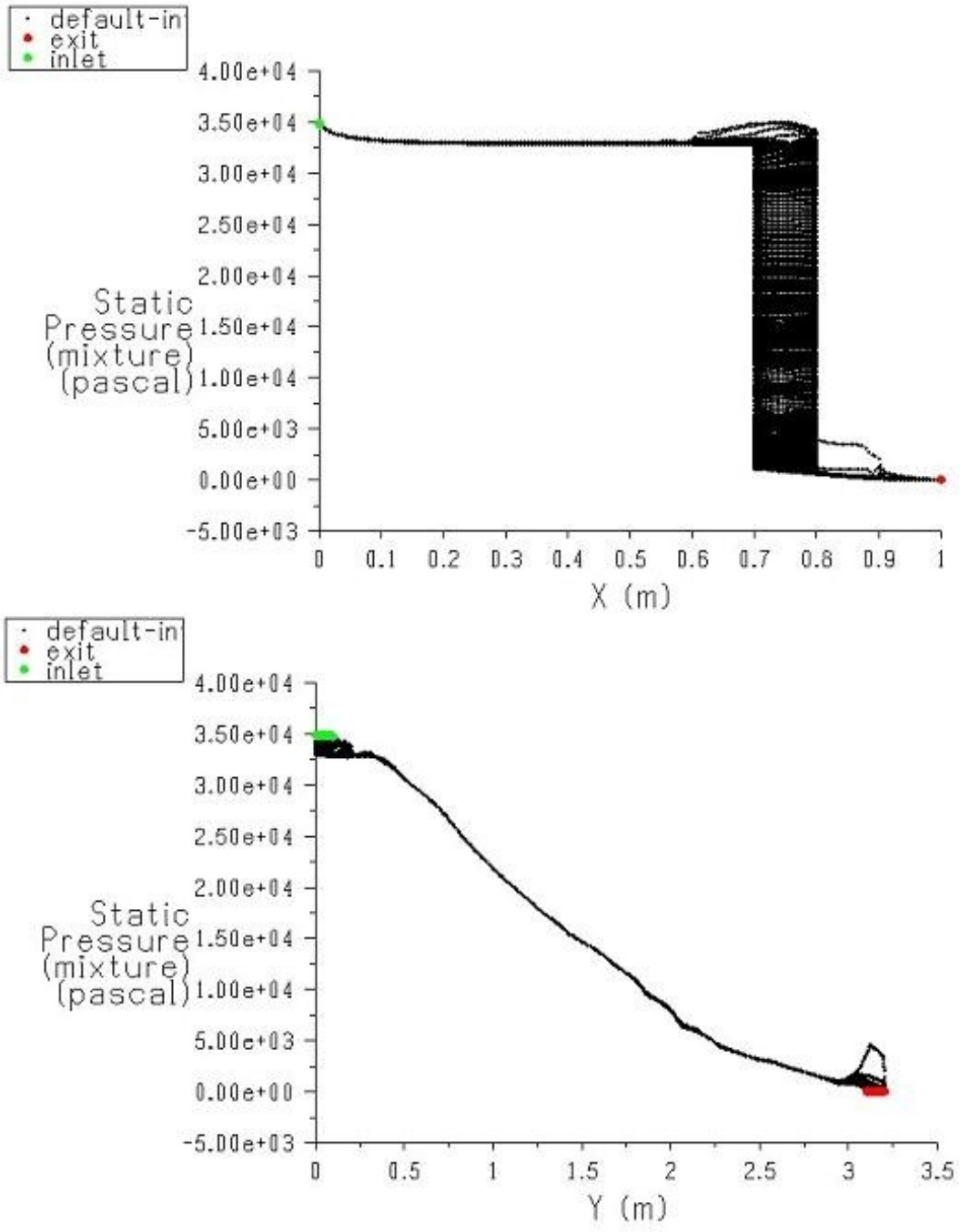

Figure 23. Static pressure of the mixture along horizontal (X) and vertical (Y) axes at time= 15.0 sec

The characteristics of the pressure drop at the riser inlet are very similar to those observed in conjunction with the steady state solution as expounded in relation with Fig. 16. However, the fluctuations in the pressure field in the vertical riser section have completely disappeared in the present unsteady state solutions. This is due to the dissipative flow properties of both air and solid particles in time. The pressure drop in the inlet section is 2.5 kPa, which amounts to 8% of the total pressure drop in the system.

The flow entering the elbow undergoes a sudden directional change which results in loss of inertia. Unlike the steady state case, no observable oscillations or fluctuations of flow properties are present in the flow field. The average value of velocity magnitude at inlet and exit is approximately 4.4 m/s, whereas the maxim value is 44.1 m/s at the inlet section of the vertical riser.

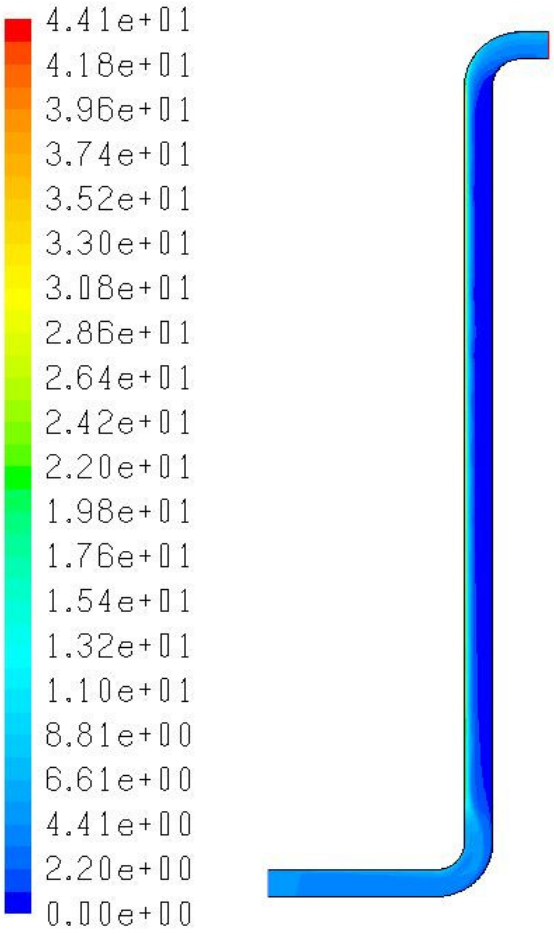

Figure 24. Contours of velocity magnitude for air (m/s) at time =15.0 seconds

Figure 25 renders enlarged views of the inlet and exit sections. When the air and solid particles mixture enter the inlet with the prescribed velocities their velocity profiles are uniform, normal to inlet surface. Inlet flow quickly forms a fully developed velocity profile in approximately 2 diameter lengths from the riser inlet then maintains the profile up to the elbow section. This velocity profile is deformed as the flow enters the vertical part of the riser section to be confined to a narrowly banded vertical high-velocity channel adjacent to the riser outer wall where most of the air mass travels downstream towards the exit. The value of the maximum velocity magnitude in this channel reaches roughly 44 m/s. This flow pattern continues until the flow is forced to go through the bend of the exit elbow. As air flow conforms to the elbow profile, the compact air flow channel disperses through the elbow section. This dispersion of the air stream aids the solid particles to scatter in the exit section.

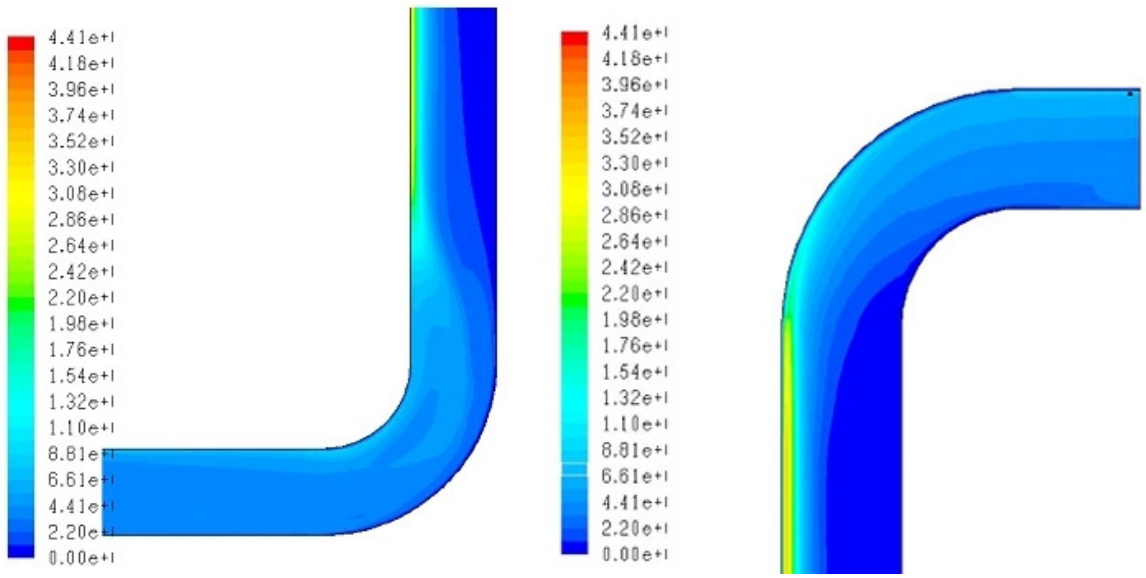

Figure 25. Contour of velocity magnitude for air (m/s)
Magnified views of inlet and exit at time =15.0 seconds.

The velocity magnitude of air versus X- and Y- Location is visualized in Fig. 26. In contrast to steady state solution results, there are no air velocity oscillations or fluctuations visible in the vertical riser section. However, the fast moving air flow channel delivers wide spectrum of air velocity magnitudes.

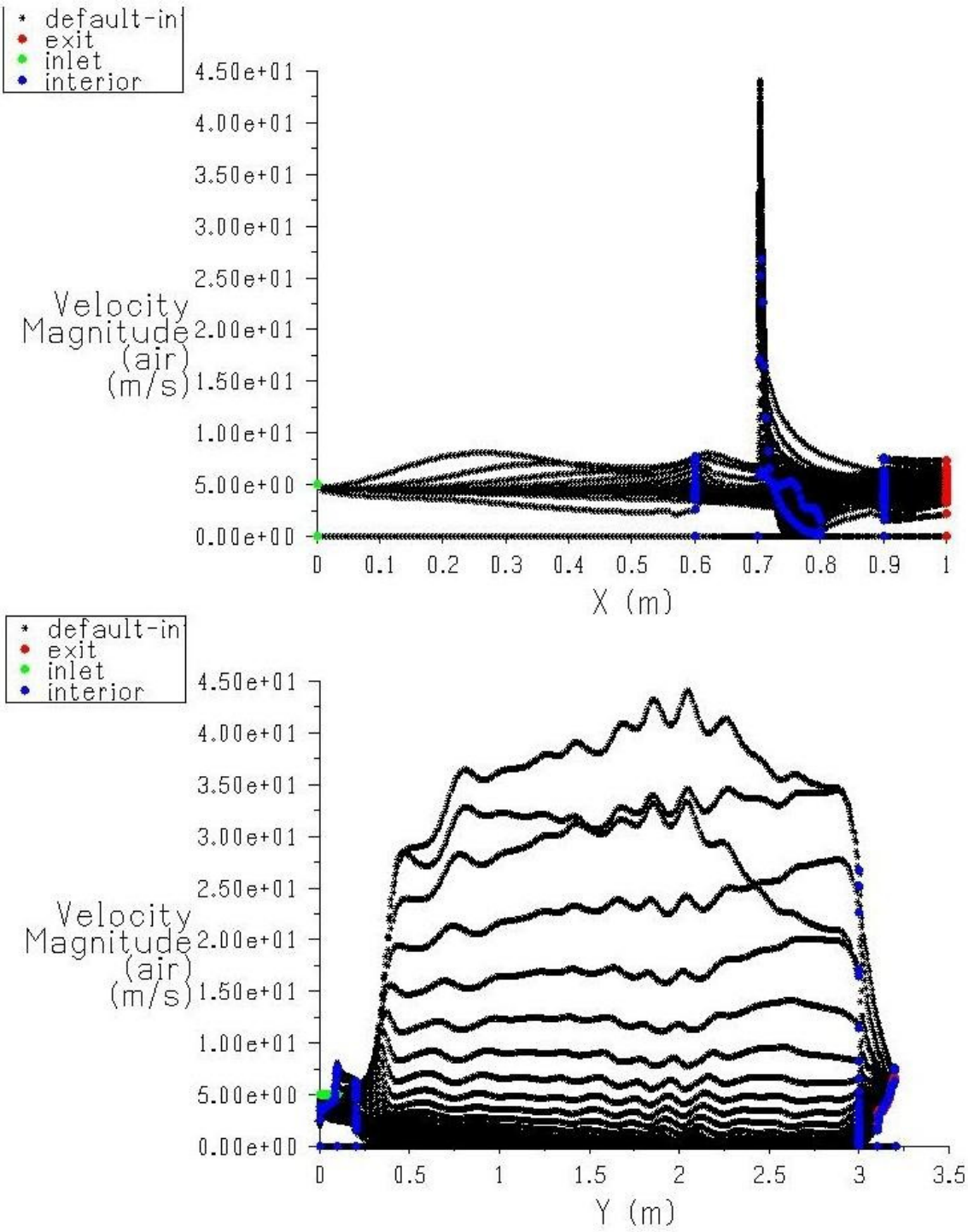

Figure 26. Velocity magnitude of air along horizontal (X) and vertical (Y) axes at time = 15.0 sec.

While most of the air mass travels through the fast moving channel, the solid particles fill the remaining volume of the vertical pipe section. Both air and particles' contour plots of volume fraction are displayed in Fig. 27.

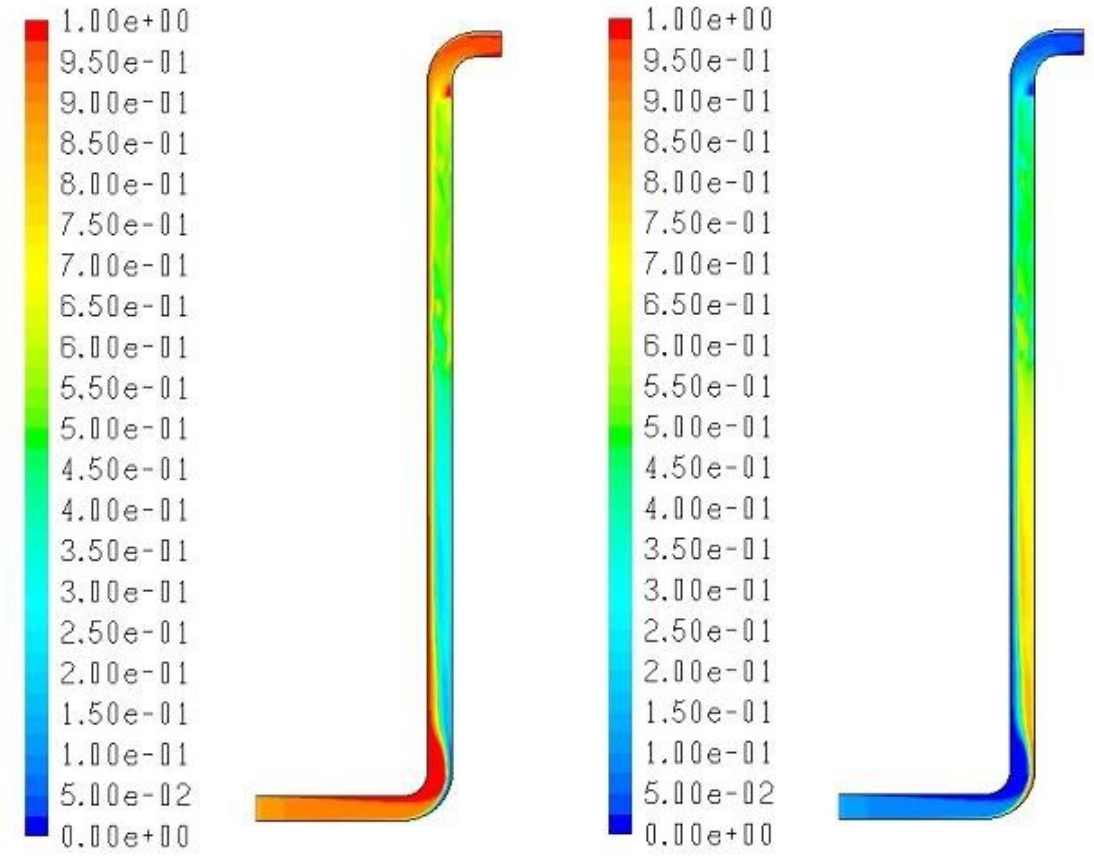

Figure 27. Contours of volume fraction for air (left) and particles (right) at 15.0 sec.

A magnified view of the inlet elbow is demonstrated in Fig. 28. It is remarked that 90% of particle volume is concentrated at the outer surface of the elbow, especially at the bend. This is the main cause of the pipeline wear and blockage for pneumatic conveying systems since the bombarding solid particles bombarding the elbow wall easily scrape off pipe material causing its erosion. It is interesting to observe that clusters of particles are formed in the riser column as indicated in Figure 29. The turbulence and restitution in the two-phase flow regime leads to interchanging events, or cycles, of cluster formation and dissipation.

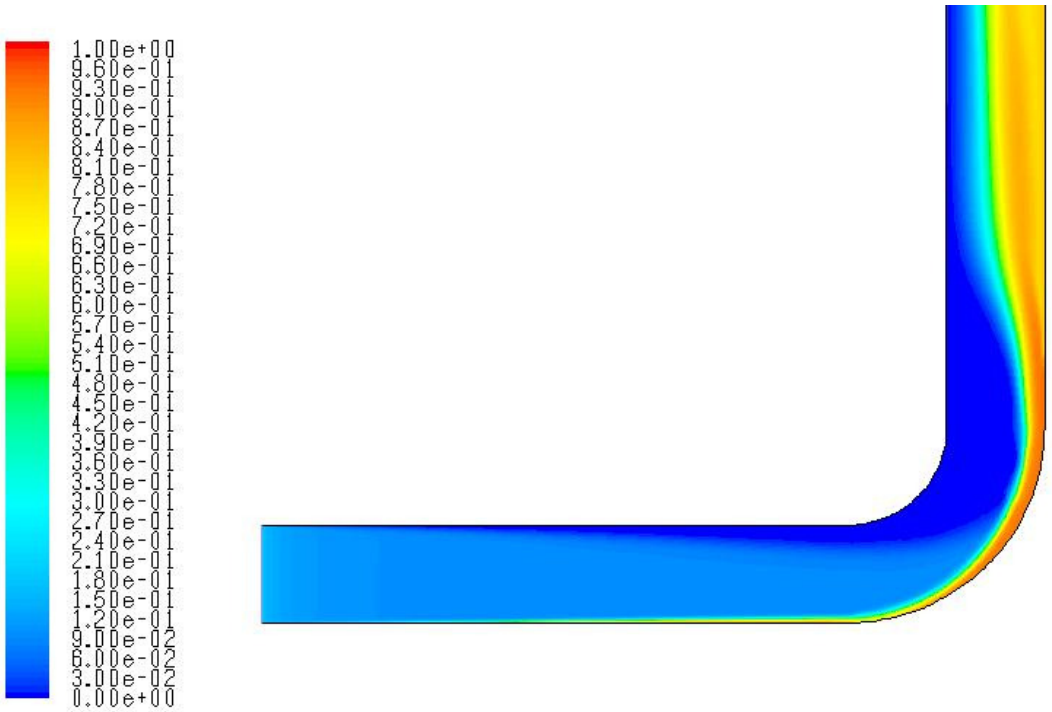

Figure 28. Contour of particles volume fraction at time = 15.0sec.

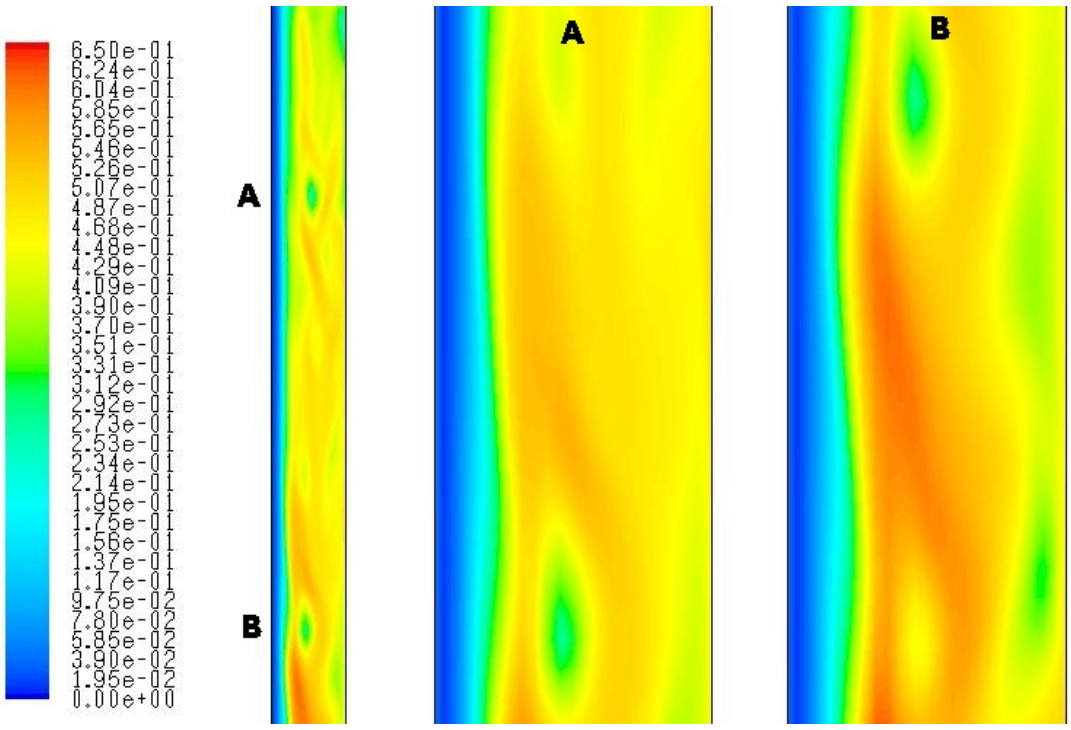

Figure 29. The Contour of particle volume fraction at time= 15.0 sec.

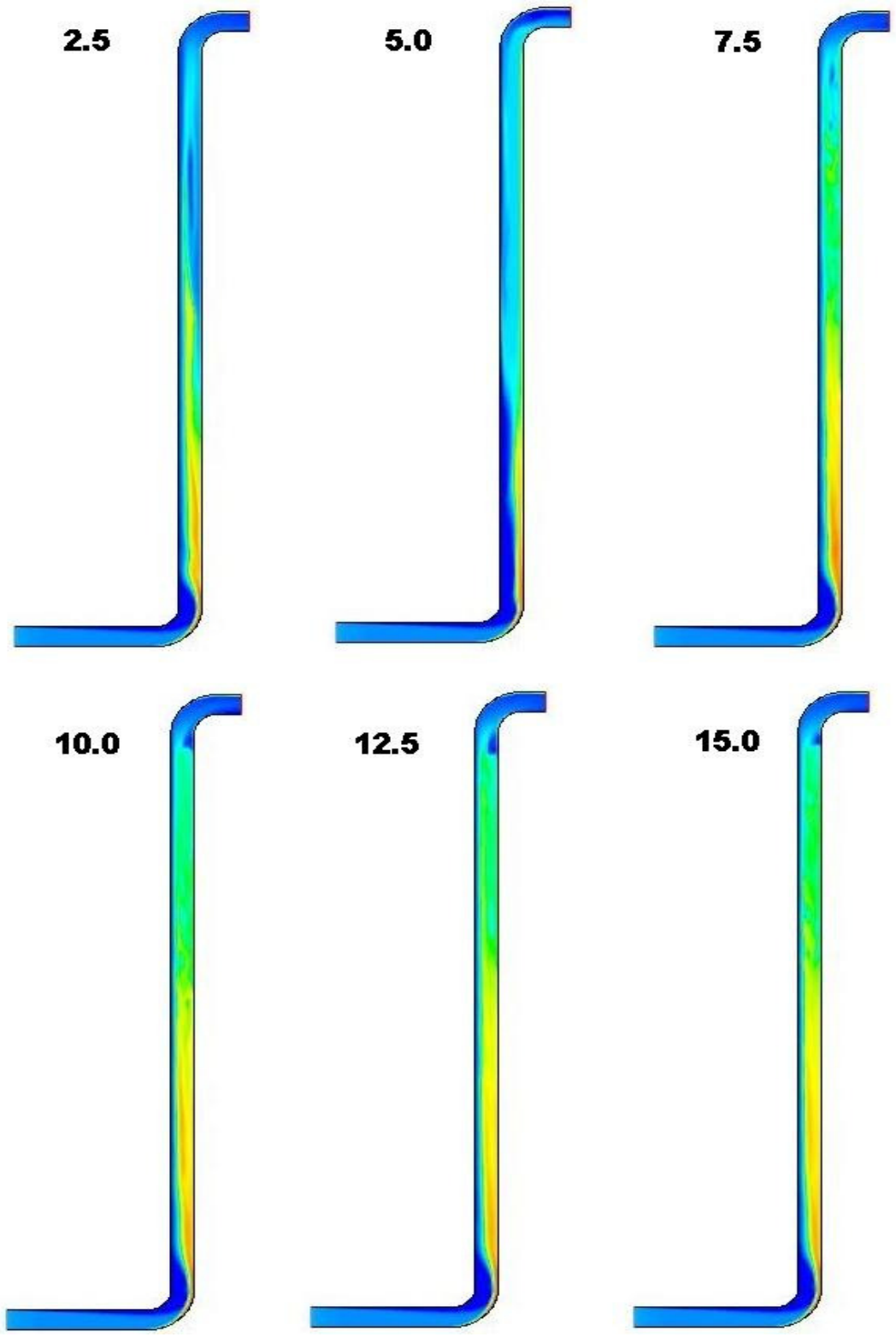

Figure 30. Volume fraction of particles at different flow times (sec)

Contours of particle volume fractions at 6 different simulation times are combined in Fig. 30. The flow reaches a pseudo steady state regime after a time of 2.0 seconds. However, irregular phenomena such as the particle clusters described in Fig. 29 abruptly disturb the flow profile. Once all of irregularly formed flow patterns are neutralized, the flow reverts to a new pseudo steady state. This is also apparent from the harmonic flow rate temporal sequence referenced in Fig. 31.

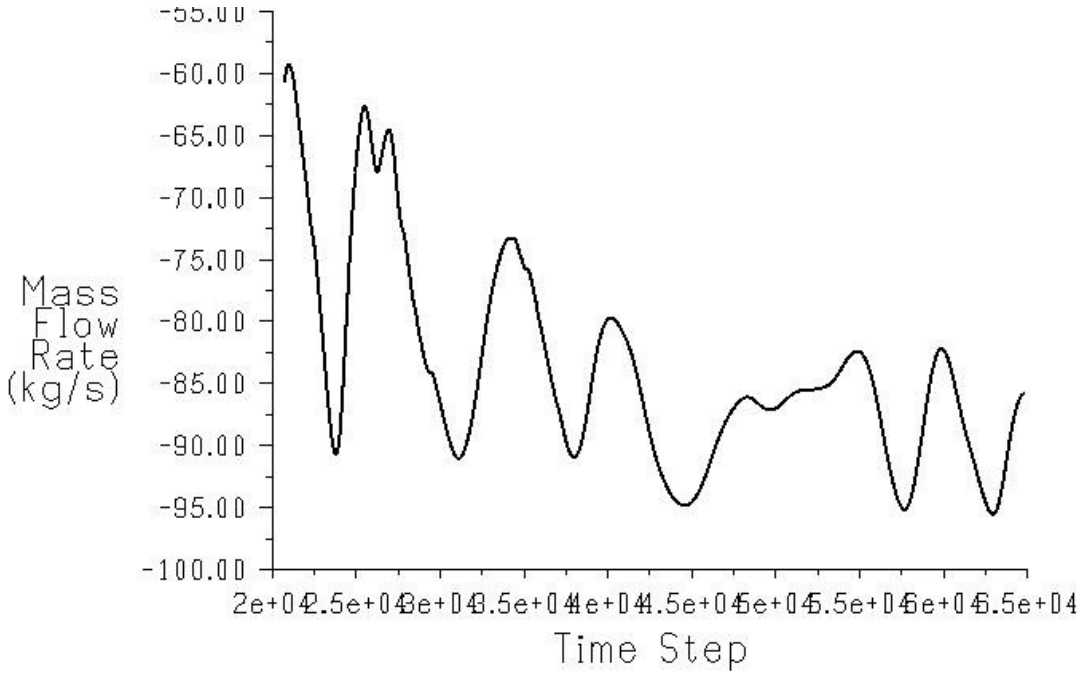

Figure 31. Convergence history of mass flow rate of air-particle mixture at riser exit at time = 16.0 sec.

The mass flow rate of air-particle mixture at riser exit surface was monitored throughout the iterations as shown in Fig. 31. While the mass flow rate at inlet remained constant at 88.5 kg/s, the mass flow rate at the exit fluctuated widely. This is mostly due to solid particles' "bursts" of accumulation and discharge observed in most two-phase gas-solid flow system. It usually takes longer time for particles to accumulate than to discharge. The frequency of accumulation-discharge is very much depends on the inlet mass flow rate and bulk density of fluid and solid particles. The mass flow rates for air and solid particle are separately calculated and listed in Table 4. Since the air to particle density ratio is 5.6e-04, the mass flow rate of air is negligible when compared to that of particles.

Table 4. Surface flux computation: Mass Flow Rate (kg/s)

	Mixture	Air	Particle
Inlet	88.4899	0.49000	88.0000
Exit	-82.1616	-0.4935	-81.6681
Net	6.32832	-0.0035	6.33185

Conclusions

1. Riser-I

Steady and unsteady state solutions are well in agreement. This is due to the relatively low air-solid particle ratio and high inlet velocities. As expected, flow separation in the elbow sections of the riser produce a large pressure drop associated with high pressure gradients and velocities. Deposition of the solid particles occurs on the outer surfaces of the elbows. The mesh type influences the convergence time but did not induce noticeable differences in the solution. For faster convergence triangular meshes could be replaced by quadratic ones. The Riser-I simplified geometry and flow conditions provided the necessary skills and knowledge to handle more realistic riser and fluidizer models.

2. Riser-II

While unsteady solutions provided more precise flow information in real time, the steady state solution defined the bounds for the flow properties in a comparably low computational cost. Thus, prior to undertaking unsteady state studies, it is recommended that steady state research on the flow model should be performed, which in turn, will be beneficial to gain insight into the problem under investigation. In addition to the observations noted with Riser I model, a cyclic phenomenon of particle clusters formation and dissipation was registered in the unsteady flow solution. The Riser II configuration resembles very closely actual risers used in industry. The model employed in Riser II is deemed to be capable of representing the physical aspects of the complex riser flow and is therefore selected as an appropriate vehicle for further research.

References

Hartge, E. U., Rensner, D., and Werther, J., "Solids Concentration and Velocity Patterns in Circulating Fluidized Beds," in Circulating Fluidized Bed Technology II, Basu, P., and Large, J. F., Eds., Permagon Press, 165-180 (1988).

Kallio, S., "Comparison of Simulated and Measured Voidage and Velocity Profiles and Fluctuations in a CFB Riser," *Proceedings of the* ***8th*** *International Conference on Circulating Fluidized Beds,* China, 105-112 (2005).

Mathiesen, V., Solberg, T., Arastoopour, H., and Hjertager, B. H., "Experimental and Computational Study of Multiphase Gas/Particle Flow in a CFB Riser," *AICHE J.*, **45**, 2503-2518 (1999).

Miller, A., and Giadspow, D., "Dense, Vertical Gas-Solid Flow in a Pipe," *AICHE J.*, **38**, 1801-1845 (1992).

Nieuwland, J. J., van Sint Annal, M., Kuipers, J.A.M., and Van Swaajj, W.P.M., "Hydrodynamic Modeling of Gas/Particle Flows in Riser Reactors", *AICHE J.*, **42**, 1569-1582 (1996).

Pugsley, T. S., Lapointe D., Hirschberg, B., and Werther, J., "Exit Effects In Circulating Fluidized Bed Risers," *Can. J. Chem. Eng.*, **75**, 1001-1010 (1997).

Tsuo, Y. P., and Giadspow, D., "Computations of Flow Patterns in Circulating Fluidized Beds," *AICHE J.*, **36**, 885-896 (1990).

Zhang, W., Tung, Y., and Johnson, F., "Radial Voidage Profiles In Fast Fluidized Beds of Different Diameters," *Chem. Eng. Sci.*, **46**, 3045-3052 (1991).

Appendix

Operating Conditions and Solver Settings

RISER-1

FLUENT
Version: 2d, pbns, eulerian, ske, unsteady (2d, pressure-based, Eulerian, standard k-epsilon, unsteady)
Release: 6.3.26
Title:

Models

Model	Settings
Space	2D
Time	Unsteady, 2nd-Order Implicit
Viscous	Standard k-epsilon turbulence model
Wall Treatment	Standard Wall Functions
Multiphase k-epsilon Models	k-epsilon Model for Each Phase
Heat Transfer	Disabled
Solidification and Melting	Disabled
Species Transport	Disabled
Coupled Dispersed Phase	Disabled
Pollutants	Disabled
Pollutants	Disabled
Soot	Disabled

Boundary Conditions

Zones

name	id	type
fluid	2	fluid
wall	3	wall
inlet	4	velocity-inlet
exit	5	pressure-outlet
default-interior	7	interior

Boundary Conditions

fluid

Condition	Value
Material Name	ash

Specify source terms?	no
Source Terms	()
Specify fixed values?	no
Fixed Values	()
Motion Type	0
X-Velocity Of Zone (m/s)	0
Y-Velocity Of Zone (m/s)	0
Rotation speed (rad/s)	0
X-Origin of Rotation-Axis (m)	0
Y-Origin of Rotation-Axis (m)	0
Deactivated Thread	no
Laminar zone?	no
Set Turbulent Viscosity to zero within laminar zone?	yes
Porous zone?	no
Porosity	1

wall

Condition	Value
Wall Motion	0
Shear Boundary Condition	0
Define wall motion relative to adjacent cell zone?	yes
Apply a rotational velocity to this wall?	no
Velocity Magnitude (m/s)	0
X-Component of Wall Translation	1
Y-Component of Wall Translation	0
Define wall velocity components?	no
X-Component of Wall Translation (m/s)	0
Y-Component of Wall Translation (m/s)	0
Wall Roughness Height (m)	0
Wall Roughness Constant	0.5
Rotation Speed (rad/s)	0
X-Position of Rotation-Axis Origin (m)	0
Y-Position of Rotation-Axis Origin (m)	0
X-component of shear stress (pascal)	0
Y-component of shear stress (pascal)	0
Specularity Coefficient	0

inlet

Condition	Value
is zone used in mixing-plane model?	no

exit

Condition	Value
Gauge Pressure (pascal)	0
Backflow Direction Specification Method	1

is zone used in mixing-plane model? no

default-interior

Condition Value

Solver Controls

Equations

Equation Solved

Flow yes
Volume Fraction yes
Turbulence yes

Numerics

Numeric Enabled

Absolute Velocity Formulation yes

Unsteady Calculation Parameters

Time Step (s) 0.00025000001
Max. Iterations Per Time Step 20

Relaxation

Variable Relaxation Factor

Pressure 0.30000001
Density 1
Body Forces 1
Momentum 0.69999999
Volume Fraction 0.2
Granular Temperature 0.2
Turbulent Kinetic Energy 0.80000001
Turbulent Dissipation Rate 0.80000001
Turbulent Viscosity 1

Linear Solver

Solver Termination Residual Reduction
Variable Type Criterion Tolerance

Pressure V-Cycle 0.1

X-Momentum	Flexible	0.1	0.7
Y-Momentum	Flexible	0.1	0.7
Volume Fraction	Flexible	0.1	0.7
Turbulent Kinetic Energy	Flexible	0.1	0.7
Turbulent Dissipation Rate	Flexible	0.1	0.7

Pressure-Velocity Coupling

Parameter	Value
Type	Phase Coupled SIMPLE

Discretization Scheme

Variable	Scheme
Momentum	Second Order Upwind
Volume Fraction	QUICK
Turbulent Kinetic Energy	Second Order Upwind
Turbulent Dissipation Rate	Second Order Upwind

Solution Limits

Quantity	Limit
Minimum Absolute Pressure	1
Maximum Absolute Pressure	5e+10
Minimum Temperature	1
Maximum Temperature	5000
Minimum Turb. Kinetic Energy	1e-14
Minimum Turb. Dissipation Rate	1e-20
Maximum Turb. Viscosity Ratio	100000

Material Properties

Material: ash (fluid)

Property	Units	Method	Value(s)
Density	kg/m3	constant	817
Cp (Specific Heat)	j/kg-k	constant	1006.43
Thermal Conductivity	w/m-k	constant	0.0242
Viscosity	kg/m-s	constant	1.7894001e-05
Molecular Weight	kg/kgmol	constant	28.966
L-J Characteristic Length	angstrom	constant	3.711
L-J Energy Parameter	k	constant	78.6
Thermal Expansion Coefficient	1/k	constant	0
Degrees of Freedom		constant	0
Speed of Sound	m/s	none	#f

Material: air (fluid)

Property	Units	Method	Value(s)
Density	kg/m3	constant	1.225
Cp (Specific Heat)	j/kg-k	constant	1006.43
Thermal Conductivity	w/m-k	constant	0.0242
Viscosity	kg/m-s	constant	1.7894e-05
Molecular Weight	kg/kgmol	constant	28.966
L-J Characteristic Length	angstrom	constant	3.711
L-J Energy Parameter	k	constant	78.6
Thermal Expansion Coefficient	1/k	constant	0
Degrees of Freedom		constant	0
Speed of Sound	m/s	none	#f

Material: aluminum (solid)

Property	Units	Method	Value(s)
Density	kg/m3	constant	2719
Cp (Specific Heat)	j/kg-k	constant	871
Thermal Conductivity	w/m-k	constant	202.4

RISER-II

FLUENT
Version: 2d, pbns, eulerian, ske, unsteady (2d, pressure-based, Eulerian, standard k-epsilon, unsteady)
Release: 6.3.26
Title:

Models

Model	Settings
Space	2D
Time	Unsteady, 2nd-Order Implicit
Viscous	Standard k-epsilon turbulence model
Wall Treatment	Standard Wall Functions
Multiphase k-epsilon Models	Dispersed Approach
Heat Transfer	Disabled
Solidification and Melting	Disabled
Species Transport	Disabled
Coupled Dispersed Phase	Disabled
Pollutants	Disabled
Pollutants	Disabled
Soot	Disabled

Boundary Conditions

Zones

name	id	type
entire	2	fluid
wall	3	wall
interior	4	interior
exit	5	pressure-outlet
inlet	6	velocity-inlet
default-interior	8	interior

Boundary Conditions

entire

Condition	Value

Material Name	particle
Specify source terms?	no
Source Terms	()
Specify fixed values?	no
Fixed Values	()
Motion Type	0
X-Velocity Of Zone (m/s)	0
Y-Velocity Of Zone (m/s)	0
Rotation speed (rad/s)	0
X-Origin of Rotation-Axis (m)	0
Y-Origin of Rotation-Axis (m)	0
Deactivated Thread	no
Laminar zone?	no
Set Turbulent Viscosity to zero within laminar zone?	yes
Porous zone?	no
Porosity	1

wall

Condition	Value
Wall Motion	0
Shear Boundary Condition	0
Define wall motion relative to adjacent cell zone?	yes
Apply a rotational velocity to this wall?	no
Velocity Magnitude (m/s)	0
X-Component of Wall Translation	1
Y-Component of Wall Translation	0
Define wall velocity components?	no
X-Component of Wall Translation (m/s)	0
Y-Component of Wall Translation (m/s)	0
Wall Roughness Height (m)	0
Wall Roughness Constant	0.5
Rotation Speed (rad/s)	0
X-Position of Rotation-Axis Origin (m)	0
Y-Position of Rotation-Axis Origin (m)	0
X-component of shear stress (pascal)	0
Y-component of shear stress (pascal)	0
Specularity Coefficient	0

interior

Condition	Value

exit

Condition	Value
Gauge Pressure (pascal)	0
Backflow Direction Specification Method	1
is zone used in mixing-plane model?	no

inlet

Condition	Value
is zone used in mixing-plane model?	no

default-interior

Condition	Value

Solver Controls

Equations

Equation	Solved
Flow	yes
Volume Fraction	yes
Turbulence	yes

Numerics

Numeric	Enabled
Absolute Velocity Formulation	yes

Unsteady Calculation Parameters

Time Step (s)	0.00025000001
Max. Iterations Per Time Step	20

Relaxation

Variable	Relaxation Factor

Pressure	0.5
Density	1
Body Forces	1
Momentum	0.2
Volume Fraction	0.60000002
Turbulent Kinetic Energy	0.80000001
Turbulent Dissipation Rate	0.80000001
Turbulent Viscosity	1

Linear Solver

Variable	Solver Type	Termination Criterion	Residual Reduction Tolerance
Pressure	V-Cycle	0.1	
X-Momentum	Flexible	0.1	0.7
Y-Momentum	Flexible	0.1	0.7
Volume Fraction	Flexible	0.1	0.7
Turbulent Kinetic Energy	Flexible	0.1	0.7
Turbulent Dissipation Rate	Flexible	0.1	0.7

Pressure-Velocity Coupling

Parameter	Value
Type	Phase Coupled SIMPLE

Discretization Scheme

Variable	Scheme
Momentum	First Order Upwind
Volume Fraction	First Order Upwind
Turbulent Kinetic Energy	Second Order Upwind
Turbulent Dissipation Rate	Second Order Upwind

Solution Limits

Quantity	Limit
Minimum Absolute Pressure	1
Maximum Absolute Pressure	5e+10
Minimum Temperature	1
Maximum Temperature	5000
Minimum Turb. Kinetic Energy	1e-14

Minimum Turb. Dissipation Rate 1e-20
Maximum Turb. Viscosity Ratio 100000

Material Properties

Material: particle (fluid)

Property	Units	Method	Value(s)
Density	kg/m3	constant	2200
Cp (Specific Heat)	j/kg-k	constant	1006.43
Thermal Conductivity	w/m-k	constant	0.0242
Viscosity	kg/m-s	constant	1.7894001e-05
Molecular Weight	kg/kgmol	constant	28.966
L-J Characteristic Length	angstrom	constant	3.711
L-J Energy Parameter	k	constant	78.6
Thermal Expansion Coefficient	1/k	constant	0
Degrees of Freedom		constant	0
Speed of Sound	m/s	none	#f

Material: air (fluid)

Property	Units	Method	Value(s)
Density	kg/m3	constant	1.225
Cp (Specific Heat)	j/kg-k	constant	1006.43
Thermal Conductivity	w/m-k	constant	0.0242
Viscosity	kg/m-s	constant	1.7894e-05
Molecular Weight	kg/kgmol	constant	28.966
L-J Characteristic Length	angstrom	constant	3.711
L-J Energy Parameter	k	constant	78.6
Thermal Expansion Coefficient	1/k	constant	0
Degrees of Freedom		constant	0
Speed of Sound	m/s	none	#f

Material: aluminum (solid)

Property	Units	Method	Value(s)
Density	kg/m3	constant	2719
Cp (Specific Heat)	j/kg-k	constant	871
Thermal Conductivity	w/m-k	constant	202.4